JOURNAL OF PETROLOGY | VOLUME 42 | NUMBER 6 | PAGES 1043–1065 | 2001

Origins of Large Volume Rhyolitic Volcanism in the Antarctic Peninsula and Patagonia by Crustal Melting

TEAL R. RILEY[1]*, PHILIP T. LEAT[1], ROBERT J. PANKHURST[1,2] AND CHRIS HARRIS[3]

[1]BRITISH ANTARCTIC SURVEY, NATURAL ENVIRONMENT RESEARCH COUNCIL, HIGH CROSS, MADINGLEY ROAD, CAMBRIDGE CB3 0ET, UK

[2]NERC ISOTOPE GEOSCIENCES LABORATORY, KEYWORTH, NOTTINGHAM NG12 5GG, UK

[3]DEPARTMENT OF GEOLOGICAL SCIENCES, UNIVERSITY OF CAPE TOWN, RONDEBOSCH 7700, SOUTH AFRICA

RECEIVED SEPTEMBER 17, 1999; REVISED TYPESCRIPT ACCEPTED JULY 10, 2000

Voluminous rhyolitic volcanism along the palaeo-Pacific margin of Gondwana was marked by three principal episodes of magmatism. The first of these (V_1) is essentially coincident with the main episode of Karoo–Ferrar magmatism at ~184 Ma. A younger (V_2) episode occurred at ~168 Ma, and a third episode (V_3) occurred in the interval 157–153 Ma. We evaluate the origin of V_1 and V_2 rhyolites from the Antarctic Peninsula using major and trace element and isotopic (Sr, Nd, O) data. An isotopically uniform ($^{87}Sr/^{86}Sr_i \sim 0{\cdot}707$; $\varepsilon Nd_i \sim -3$) andesite–dacite magma was generated as a result of anatexis of 'Grenvillian age' hydrous mafic lower crust, linked to earlier, arc-related underplating. The lower-crustal partial melts would have mixed with fractionated components of the mafic underplate, followed by subsequent storage and homogenization. Early Jurassic (V_1) rocks of the southern Antarctic Peninsula are interpreted as melts of upper-crustal paragneiss, which have mixed with the isotopically uniform magma in upper-crustal magma chambers. The V_2 rhyolites are the result of assimilation–fractional crystallization of the isotopically uniform magma. This occurred in upper-crustal magma chambers involving assimilants with similar isotopic composition to that of the magma. A continental margin setting was crucial in developing hydrous, readily fusible lower crust. Lower-crustal anatexis was in response to mafic underplating associated with the Discovery–Shona–Bouvet group of plumes, thought to be responsible for the Karoo magmatic province. The progression (old to young) of volcanism from NE to SW in Patagonia and south to north in the Antarctic Peninsula is consistent with migration away from the mantle plumes towards the proto-Pacific margin of Gondwana during rifting and break-up.

KEY WORDS: *crustal contamination; Gondwana; MASH; rhyolite; Sr–Nd–O isotopes*

INTRODUCTION

Petrogenetic models to explain the generation of silicic magmas fall into two broad categories. The first is where silicic magmas are derived from a basaltic parent magma by fractional crystallization or assimilation combined with fractional crystallization (AFC). This process is often suggested for small magma batches, because to generate large volumes of silicic magma, unreasonably large amounts of basalt must be crystallized. The second model, in which basaltic magmas provide heat for the partial melting of crustal rocks, is considered more appropriate for larger volume silicic magma bodies.

Large volume rhyolite provinces (>10^3 km^3) are reported from a variety of tectonic settings, including continental margins, continental rifts, and continental interiors associated with mantle plume-derived magmatism. Voluminous silicic magmatism associated with subduction at continental margins is documented from several regions, e.g. Sierra Madre Occidental, Mexico (Cameron *et al.*, 1980), the Andes (Hildreth & Moorbath, 1988) and Taupo, New Zealand (McCulloch *et al.*, 1994). Although associated with mafic rocks, silicic rocks dominate these provinces. Ewart *et al.* (1992) have documented

*Corresponding author. Telephone: (+44) 1223 221423. Fax: (+44) 1223 362616. E-mail: t.riley@bas.ac.uk

Extended dataset can be found at http://www.petrology.oupjournals.org

large volume rhyolitic magmatism from Queensland (Australia), which has many features of continental margin volcanism, but has been attributed to continental rifting during break-up of eastern Gondwana in the Cretaceous. Other large volume rhyolites occur in continental interiors and are associated both chronologically and spatially with large volume flood basalt provinces, which may be associated with mantle plumes (e.g. Lebombo, Cleverly *et al.*, 1984; Paraná–Etendeka, Garland *et al.*, 1995).

The voluminous rhyolites (~235 000 km^3; Pankhurst *et al.*, 1998) of the Chon Aike Province (South America–Antarctic Peninsula) were emplaced over ~30 my (Early Jurassic–Late Jurassic), during three main episodes of magmatism (Pankhurst *et al.*, 2000). Pankhurst & Rapela (1995) attributed the origin of the Chon Aike rhyolites to partial melting of Grenvillian mafic, granulite-facies lower crust to produce parental andesite and dacite magmas, which then evolved to rhyolite by fractional crystallization. Nevertheless, volcanic rocks from the entire province show large variations, not only in age, but also in chemistry and geological setting, and Pankhurst *et al.* (1998) suggested that a single petrogenetic model for the entire province is unlikely. These workers proposed that both lithospheric extension, related to Gondwana break-up and the impact of a mantle plume, and subduction along the palaeo-Pacific margin may have been important in producing tectonic conditions favourable for the generation and emplacement of the silicic volcanic rocks.

GEOLOGICAL SETTING

Regional setting

Evidence of a magmatic mega-province emplaced at ~182 Ma (Duncan *et al.*, 1997) in pre-break-up reconstructions of Gondwana is recorded in the volcanic rocks of southern Africa, SE Australia, New Zealand, Tasmania and Antarctica (Storey & Kyle, 1997; Fig. 1a). These provinces are dominantly mafic and their origins can be linked to intracontinental lithospheric extension related to early stages of continental break-up, and probable impact of one or more mantle plumes (White & McKenzie, 1989; Cox, 1992; Storey & Kyle, 1997).

The major silicic portion of pre-break-up Gondwana magmatism is exposed in the Patagonian region of South America. The dominant Patagonia formations are collectively called the Chon Aike Province (Pankhurst *et al.*, 1998). These volcanic rocks are predominantly pyroclastic, dominated by ignimbrites of rhyolitic composition (Pankhurst *et al.*, 1998). Jurassic volcanic rocks exposed along the east coast of the Antarctic Peninsula are also dominated by rhyolitic ignimbrite flows, with individual units up to 80 m in thickness, and a total thickness of ~1 km (Riley & Leat, 1999).

Jurassic silicic volcanic rocks of the Antarctic Peninsula

This paper documents the geochemistry of the Jurassic silicic volcanic rocks of the Antarctic Peninsula, and discusses their relationship to those of Patagonia.

With the exception of Cenozoic volcanic rocks associated with the slowing and cessation of subduction (Hole, 1988), Thomson & Pankhurst (1983) assigned all volcanic rocks in the Antarctic Peninsula to the Antarctic Peninsula Volcanic Group (APVG; Jurassic–Cenozoic), which is regarded as the product of magmatic arc volcanism at the palaeo-Pacific margin (Storey & Garrett, 1985). Along the eastern side of the Antarctic Peninsula, thick (up to 1 km) dominantly silicic volcanic rocks crop out, and are typically Middle Jurassic in age (Riley & Leat, 1999). The silicic volcanic rocks of the east coast are associated with comagmatic granitoid plutons of Early–Middle Jurassic age (Leat *et al.*, 1995) and thick sequences of sedimentary rocks, which have a characteristic continental affinity (Riley & Leat, 1999). These Mesozoic sequences rest unconformably upon Permian–Triassic quartzose metasedimentary rocks of the Trinity Peninsula Group (Smellie *et al.*, 1996).

Mapple Formation

The region around Cape Disappointment (Fig. 1b) has the most widespread occurrence of silicic volcanic rocks in the Antarctic Peninsula. Ignimbrite units dominate (~85%) the Mapple Formation and exhibit a diverse range in their degree of welding and lithic content. The volcanic rocks are almost entirely subaerial, although localized subaqueous emplacement has been identified (Riley & Leat, 1999). Ignimbrite depositional units are typically 5–20 m in thickness, exceptionally reaching 80 m, and the entire sequence has a maximum observed thickness of ~1 km in the Mapple Glacier region, where the Mapple Formation is defined (Riley & Leat, 1999). The ignimbrites are intercalated with minor air-fall units, lag breccias and lava flows. The Mapple Formation was metamorphosed and deformed, probably during the end-Jurassic Palmer Land compressional event (Kellogg & Rowley, 1989). Metamorphic grade ranges up to greenschist facies in the western part of the outcrop and associated deformation generated open folds and low-angle faults. Steeply dipping cleavage has developed in epiclastic and many mudflow deposits, and increases in intensity westward.

The ignimbrite units are generally phenocryst poor, with an assemblage of embayed quartz, K-feldspar, plagioclase, biotite, magnetite, apatite, orthopyroxene,

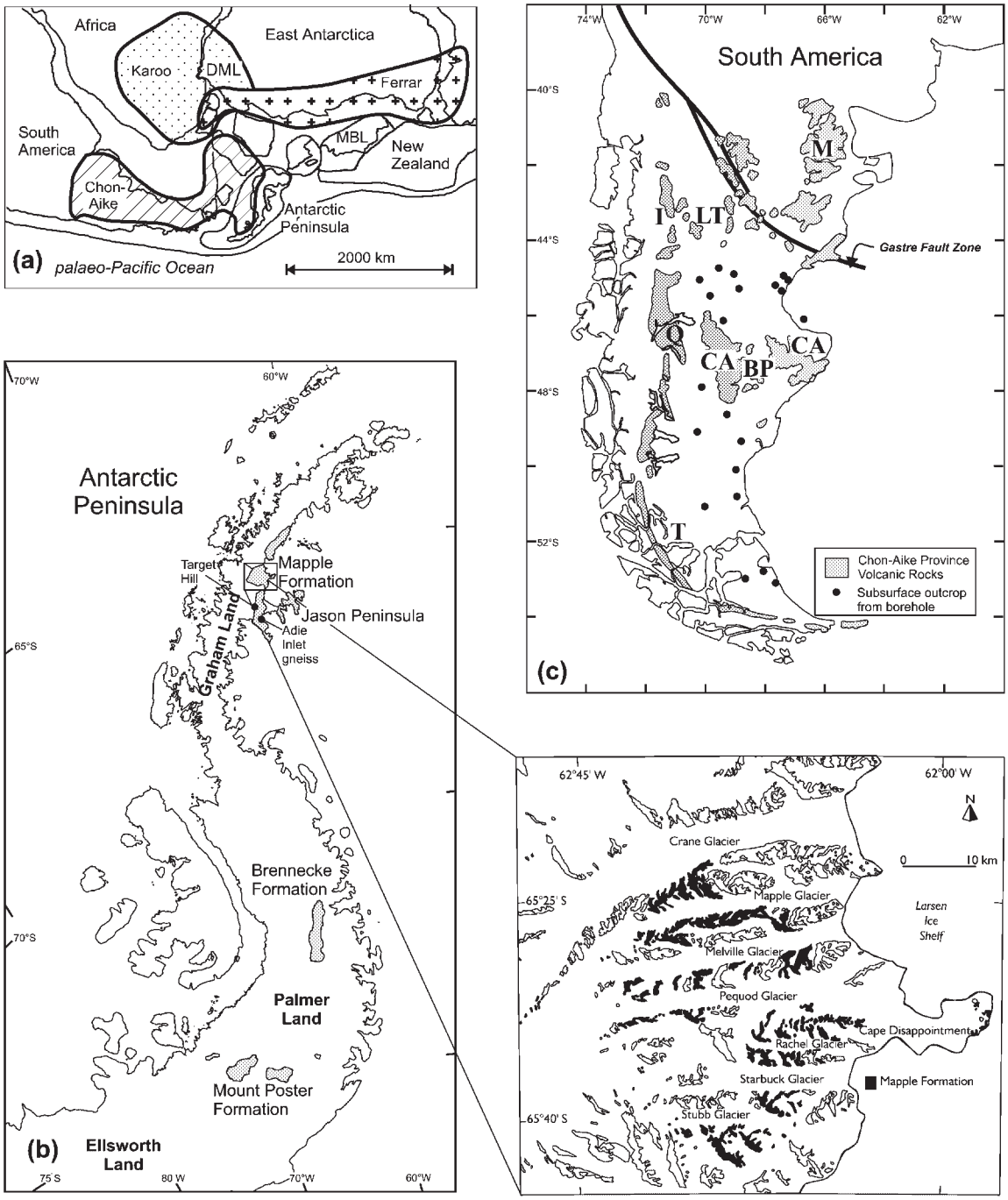

Fig. 1. (a.) Reconstruction of pre-break-up western Gondwana showing the major magmatic provinces (Karoo, Ferrar and Chon Aike), after Storey *et al.* (1992). MBL, Marie Byrd Land; DML, Dronning Maud Land. (b) Map of the Antarctic Peninsula showing the extent of the Mapple, Mount Poster and Brennecke formations. Inset is outcrop extent of the Mapple Formation with locality names. (c) The Jurassic Chon Aike volcanic province of Patagonia showing extent of outcrop and subsurface exposures. Individual formations: M, Marifil; LT, Lonco-Trapial; I, Ibañez; Q, El Quemado; CA, Chon Aike; BP, Bajo Pobre; T, Tobífera (after Pankhurst *et al.*, 1998).

titanite, rutile and zircon. The feldspar is extensively altered and replaced by calcite, sericite and clay minerals. Biotite is also altered and typically replaced by chlorite. The development of spherulites (axiolitic and spherical) as a result of high-temperature devitrification of glass is widespread in the rhyolitic ignimbrites.

Silicic volcanic rocks believed to be a continuation of the Mapple Formation are widely exposed on Jason

Peninsula (Fig. 1b). The geology is dominated by relatively flat-lying rhyolitic ignimbrites and lava flows, which are mineralogically similar to the rhyolites of the Mapple Formation. Rare mafic to intermediate lavas and sills, which were believed to form a bimodal assemblage with the silicic rocks (Smellie, 1991) are now thought to be Late Jurassic in age, related to the formation of the Latady basin (Riley *et al.*, 1997; Riley & Leat, 1999).

Mount Poster Formation

The Mount Poster Formation crops out in eastern Ellsworth Land, southern Antarctic Peninsula (Fig. 1b), and comprises rhyolitic pyroclastic rocks and lava flows. The volcanic sequence has a minimum thickness of 500 m and locally reaches ~1 km. The total thickness of the formation has been estimated at ~2 km (Rowley *et al.*, 1982). The formation is dominated by a monotonous succession of crystal-rich, grey or black welded ignimbrite units and minor lava flows. In strongly welded units, fiamme are only weakly discernible, but poorly welded ignimbrites contain oblate, crystal-rich pumices, which account for up to 20% of the rock. At one locality, strongly welded ignimbrite units with pumice flattening ratios of up to 10:1 occur in association with rheomorphic ignimbrites, which have a well-defined parataxitic texture. An intracaldera setting for the volcanic rocks is suggested by the lithological homogeneity and dense welding of most of the ignimbrites, the thickness of the succession, the pervasive low-grade alteration, and faulting and dyke emplacement at the putative caldera margins (Riley & Leat, 1999). Such features are characteristic of intracaldera ignimbrite-dominated successions from the western USA (Lipman, 1984) and Alaska (Bacon *et al.*, 1990).

Petrographically, the rhyolites contain abundant phenocrysts of plagioclase, sanidine, hornblende, embayed quartz, and Fe–Ti oxides, with an alteration assemblage of sericite, clay minerals and calcite. The rhyolites of the Mount Poster Formation have all undergone chlorite-grade metamorphism (Rowley *et al.*, 1982). The ignimbrites have an apparent porphyritic texture, comprising abundant feldspar crystals, which occur as single euhedra or as clusters.

Brennecke Formation

The Brennecke Formation comprises silicic metavolcanic units, which crop out at several localities in eastern Palmer Land (Fig. 1b). At the type locality (Kamenev Nunataks) a sequence of massive rhyolitic lava flows are interbedded with more foliated, welded pyroclastic rocks and black shales. The rhyolites may be contemporaneous with an ~150 m thick succession of basaltic lavas (Hjort Formation), perhaps forming a bimodal association (Wever & Storey, 1992).

Jurassic silicic volcanism of Patagonia (Chon Aike Province)

The silicic Chon Aike province of Patagonia (Fig. 1c) extends from the Atlantic coast to the Chilean side of the Andes and is correlated with the Jurassic silicic volcanic rocks of the Antarctic Peninsula. In eastern Patagonia, the volcanic rocks are predominantly flat lying and undeformed where they overlie crystalline basement rocks of Precambrian to earliest Jurassic age and, locally, Liassic rift-related sedimentary rocks. In contrast, silicic volcanic rocks of the Andean Cordillera form relatively narrow outcrops, which are locally deformed, tilted and strongly affected by hydrothermal alteration.

The province is dominated by poorly welded, phenocryst-poor ignimbrites, for which source calderas (e.g. Aragón *et al.*, 1996) have been identified locally. These relationships imply that the silicic magmas were erupted from magma chambers situated within the upper crust. The province is chemically dominated by rhyolite, although it exhibits consistent bimodality between rhyolite and andesite–basaltic andesite.

The Chon Aike Province comprises several formations, which have been fully documented by Pankhurst *et al.* (1998). The Early Jurassic Marifil Formation and the Middle Jurassic Chon Aike Formation are summarized below.

Chon Aike Formation

The Chon Aike Formation covers an area of some 100 000 km^2 in the Deseado Massif (Fig. 1c) and locally reaches a thickness of ~300 m. Pyroclastic rocks predominate with ignimbrites forming ~85% of the outcrop, with subordinate epiclastic deposits, air-fall tuffs and intercalated lavas. Modally, the ignimbrites are phenocryst-poor rhyolites or leucocratic dacites, with vitroclastic, eutaxitic and pseudofluid textures according to the degree of welding. The principal phenocrysts are quartz, K-feldspar, plagioclase and biotite; accessories are magnetite, ilmenite, apatite and monazite. The alteration assemblage is quartz, sericite, calcite, albite and clay minerals. Alteration of the rhyolites is widespread, and often obvious from the pervasive pink to dark red colour of the rocks that results from oxidation of finely disseminated Fe-sulphide.

Marifil Formation

The Marifil Formation is also dominated by pyroclastic deposits, relative to tuffs and lavas, which account for <10% of the outcrop. Ignimbrites form cooling units up to 100 m thick, in which welding is often strong, and commonly have a massive red–brown aspect. The ignimbrites cover an area of >50 000 km^2 in the east of the Marifil Formation, where they form flat-lying sheets.

Tuffs, lapilli-tuffs and volcanic agglomerates are interbedded with the ignimbrites, and the sequence is cut by sub-volcanic intrusions, including dacitic and andesitic dykes, which, according to their isotopic composition, are comagmatic with the ignimbrites (Rapela & Pankhurst, 1993). Clastic sedimentary intercalations in the Marifil Formation are much less common than in the Chon Aike Formation.

GEOCHRONOLOGY

The chronology of eruption of the silicic volcanic rocks of Patagonia and the Antarctic Peninsula has been recently established, largely through the use of U–Pb ion microprobe dating (Pankhurst *et al.*, 2000) and $^{40}Ar/^{39}Ar$ geochronology (Féraud *et al.*, 1999). These new data suggest that volcanism continued over at least 30 my, from Early Jurassic to Late Jurassic, but with three principal episodes representing the most intense phases of activity. The first of these (termed V_1, 188–178 Ma) includes eruption of the Marifil Formation of NE Patagonia and the Brennecke and Mount Poster formations of the southern Antarctic Peninsula. The rhyolites of the Marifil Formation have an age range of 188–178 Ma, with a peak at 184 $\pm$ 2 Ma. Although this range is produced from Rb–Sr geochronology (Pankhurst & Rapela, 1995; Pankhurst *et al.*, 2000), a very similar age range is provided by $^{40}Ar/^{39}Ar$ geochronology (Féraud *et al.*, 1999). The Brennecke Formation of southern Antarctic Peninsula has yielded a U–Pb SHRIMP age of 184 Ma (Pankhurst *et al.*, 2000) indicating a contemporaneous event to the Marifil Formation. This event also extends to the Mount Poster Formation, which has yielded U–Pb SHRIMP ages of 189 $\pm$ 3 and 188 $\pm$ 3 Ma (Fanning & Laudon, 1999) from the silicic rocks. There is also evidence of zircon inheritance at $\sim$185 Ma in younger granitoids and volcanic rocks of the Antarctic Peninsula (Fanning & Laudon, 1999; Pankhurst *et al.*, 2000), which suggests that V_1 volcanic rocks may be more widespread at depth than indicated by the present outcrop. A younger age of 168 $\pm$ 3 Ma has also been recorded from the Mount Poster Formation (Fanning & Laudon, 1999), which is anomalous with respect to the age of other volcanism from the southern Antarctic Peninsula. However, given the consistency of an Early Jurassic age for most of the volcanism, an approximate age of 185 Ma will be assumed for the Marifil, Brennecke and Mount Poster formations. The age range of the V_1 episode brackets the sharp peak of flood basalt volcanism at $\sim$182 Ma in the Karoo and Ferrar provinces.

The second episode (V_2) occurred over the interval 172–162 Ma and includes the major part of the Chon Aike Formation and the entire known outcrop of the Mapple Formation. The Tobífera Formation of southernmost Patagonia yielded ages of 178 and 171 Ma (Pankhurst *et al.*, 2000) and may partly span the interval between V_1 and V_2. The Mapple Formation has yielded four high-precision SHRIMP ages of 168–171 Ma, whereas the Chon Aike Formation has a grouping of ages at 168–169 Ma (Pankhurst *et al.*, 2000), therefore an age of 168 Ma will be used throughout this paper for these formations.

The final episode, V_3 (157–153 Ma), is confined to the Andean volcanic outcrops of the El Quemado Formation (Argentina) and Ibañez Formation (Chile), although small granite bodies of this age occur both in western Patagonia and in the western Antarctic Peninsula, and may be subvolcanic equivalents.

The progression of the three silicic episodes shows east–west migration of volcanism in Patagonia and south–north migration in the Antarctic Peninsula. Pankhurst *et al.* (2000) argued that, viewed in the context of pre-breakup Gondwana, this geographical pattern corresponds both in space and in time to migration of magmatism away from the postulated site of the Discovery–Shona–Bouvet group of mantle plumes towards the proto-Pacific margin of the supercontinent. It was noted that this was also consistent with the change from chemically intraplate silicic magmatism represented by the V_1 event, to the more strongly subduction-related character of the V_2 and V_3 rhyolites. This changing character, and its petrogenetic interpretation, is investigated in more detail here.

GEOCHEMISTRY

Detailed geochemical data from two Antarctic Peninsula formations are presented in this paper: the Mount Poster Formation (Early Jurassic; V_1) and the Mapple Formation (Middle Jurassic; V_2). Comparisons are made with previously published data from the Chon Aike (V_2) and Marifil (V_1) formations of Patagonia (Pankhurst *et al.*, 1998), and the Brennecke Formation (V_1) of the Antarctic Peninsula (Wever & Storey, 1992).

Analytical techniques

Rb–Sr whole-rock analyses were carried out at the NERC Isotope Geosciences Laboratory, Keyworth. Rb/Sr ratios were determined by X-ray fluorescence (XRF); precision is $\pm$0·5% (1σ) for concentrations >50 ppm. Sr and Nd isotope compositions were determined on a Finnegan-MAT 262 mass-spectrometer using static multichannel collection, to an internal precision of better than 10 ppm (1 SEM). The $^{87}Sr/^{86}Sr$ ratios were further normalized to a nominal value of 0·710235 for the NBS987 standard (which gave a mean value of 0·710183 $\pm$ 15 during this

study) to allow for long-term drift in collector efficiencies. Long-term reproducibility of $^{143}Nd/^{144}Nd$ ratios both on the La Jolla (mean value of 0·511900 ± 8 during this study) and in-house standards is better than 15 ppm (1σ). Sm/Nd ratios on rock standards are reproducible to 0·1–0·2% (1σ). εNd values were calculated using values of 0·1966 and 0·512638 for the $^{147}Sm/^{144}Nd$ and $^{143}Nd/^{144}Nd$ ratios of the chondritic reservoir (CHUR), respectively.

Oxygen isotope data were obtained at the University of Cape Town for handpicked quartz phenocrysts to ensure that no secondary quartz was analysed. The quartz phenocrysts were cleaned in warm dilute HF to remove any glass, carbonate and feldspar. Full analytical procedures have been detailed by Harris & Erlank (1992).

Major and selected trace element analysis was by standard XRF techniques at the Department of Geology, University of Keele, with methods fully detailed by Floyd (1985).

Higher precision trace element abundances were determined by inductively coupled plasma mass spectrometry (ICP-MS) at the University of Durham. To ensure complete dissolution of the silicic rocks, fused glass beads rather than powdered samples were used. The glass beads were prepared using a Li-borate flux, crushed and dissolved by standard acid ($HF–HNO_3$) digestion. The analytical methods, precision and detection limits are comparable with those detailed by Pearce *et al.* (1995*a*).

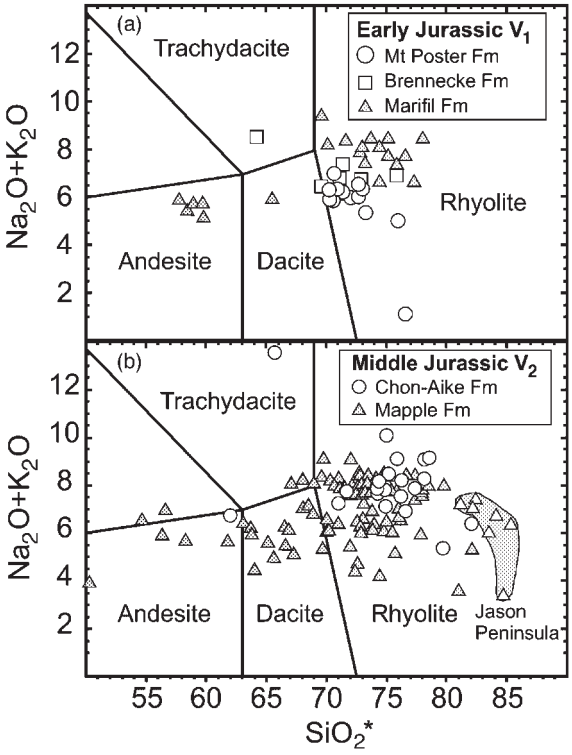

Fig. 2. Total alkali vs SiO_2 plot for the Early and Middle Jurassic rocks of the Antarctic Peninsula (this study) and Patagonia (Pankhurst *et al.*, 1998). SiO_2 is recalculated to volatile-free totals of 100% (SiO_2*). A full dataset is available from the *Journal of Petrology* Web site at http: www.petrology.oupjournals.org.

Alteration

Rhyolitic rocks are susceptible to element mobility during low-grade metamorphism, hydrothermal activity and low-temperature hydration. These processes typically result in the mobility of some major elements (e.g. Si, Na, K, Ca) and the large ion lithophile elements (LILE), Rb, Ba and Sr. The high field strength elements (HFSE), Ti, P, Th, Zr, Nb, Hf, Y and the rare earth elements (REE) are generally immobile during these alteration processes. Therefore, many of the petrogenetic interpretations will concentrate upon the HFSE and REE, which can be assumed to be present in original magmatic proportions.

Low-temperature hydration

The low-temperature hydration and devitrification of rhyolite glass is commonly associated with an increase in K, loss of Na, mobility of SiO_2 and oxidation of Fe (Stewart, 1979). Alteration is most evident on Jason Peninsula, where many of the rhyolites have SiO_2 contents in excess of 78 wt % SiO_2 (the maximum for fresh rhyolite glass), with values up to 87 wt % (see Fig. 3a, below). They are also characterized by very high concentrations of K_2O (~7–9%) relative to 3–5% for the less altered rhyolites. Conversely, Na_2O levels are very low in the Jason Peninsula rhyolites, typically ≪1%, relative to values of 3–4% in unaltered rhyolites. Rhyolites from Jason Peninsula are also characterized by red coloration, resulting from the oxidation of Fe.

Hydrothermal alteration

Hydrothermal alteration of silicic rocks is commonly associated with enrichment in K, Rb, Ba, Si and S, coupled with relative depletion in Na, Ca and Sr (e.g. Howells *et al.*, 1991). Some of the Mapple Formation rhyolites record relatively high levels of K_2O, SiO_2 and S (especially Jason Peninsula), but not Ba and Rb. There are also relative depletions in CaO and Na_2O. This is consistent with hydrothermal alteration, but the effects are similar to those associated with low-temperature hydration and regional metamorphism.

Burial and regional metamorphism

The Mapple Formation is interpreted to have undergone regional metamorphism, possibly during the Palmer Land deformation event (~150 Ma; Kellogg & Rowley, 1989).

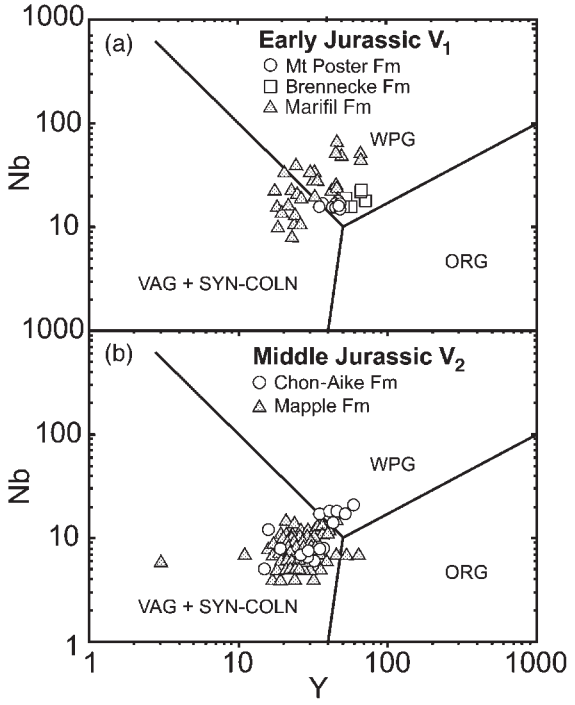

Fig. 3. Nb–Y discrimination plots for silicic rocks from the Antarctic Peninsula and Patagonia. The fields characteristic of within-plate granites (WPG), ocean ridge granites (ORG) and volcanic arc–syncollisional granites (VAG + SYN-COLN) are those defined by Pearce *et al.* (1984).

K, Sr, Rb and Ba are all considered to be highly mobile during regional metamorphism (Thorpe *et al.*, 1993); however, Sr isotope ratios are very uniform throughout the Mapple Formation and yield Rb–Sr isochrons (e.g. Pankhurst, 1982) comparable with the U–Pb SHRIMP data, suggesting that Sr has been largely unaffected by regional metamorphism.

Classification of volcanic rocks

The Jurassic volcanic rocks from the Antarctic Peninsula and Patagonian South America are predominantly silicic (>70% SiO_2). Mafic compositions are rare or absent in the formations discussed within this paper; however, the contemporaneous Lonco–Trapial and Bajo Pobre formations of Patagonia (Fig. 1c) are dominated by intermediate compositions (Pankhurst *et al.*, 1998). Rare intermediate rocks are present within the Marifil Formation, but the province is dominated by rhyolites, with SiO_2 compositions between 70 and 76 wt % and $Na_2O + K_2O$ of 6–9 wt %. The Mount Poster and Brennecke formations of the southern Antarctic Peninsula are entirely silicic (Fig. 2a), although the neighbouring Hjort Formation of mafic greenstones is considered to be contemporaneous with the Brennecke Formation (Wever & Storey, 1992).

The Middle Jurassic rocks of the Mapple and Chon Aike formations are also dominated by strongly silicic compositions (Fig. 2b), with mafic to intermediate rocks virtually absent from both formations. Pankhurst *et al.* (1998) made general observations on the geochemistry of the Chon Aike Province rhyolites and discriminated between groups on the basis of immobile trace element abundances. On the basis of Nb and Y abundances, discriminations could be made between the younger (~154 Ma; V_3 group) formations of the Andean margin and the V_1 and V_2 events located toward the continental interior. In general terms, the Andean margin formations (Ibañez, El Quemado, Tobífera; Pankhurst *et al.*, 1998), the Mapple Formation and parts of the Chon Aike Formation have low Nb (<12 ppm) contents, characteristic of rhyolites in a continental margin setting. The rhyolites from the Marifil, Chon Aike (in part), Brennecke and Mount Poster formations have higher Nb (~20 ppm) contents (Fig. 3a and b), typical of rhyolites in a continental interior setting (Macdonald *et al.*, 1992).

Early Jurassic volcanic rocks (V_1) of the Mount Poster Formation

Major element geochemistry

Analyses of the Mount Poster Formation are listed in Table 1 and their range is illustrated in an SiO_2–TiO_2 plot (Fig. 4a). The most striking observation is the occurrence of two groups; a high-Ti group (>0·7 wt % TiO_2), at 70–74 wt % SiO_2, and a low-Ti group (<0·4 wt % TiO_2), at >76 wt % SiO_2. The grouping corresponds to geological setting, with the higher-Ti group occurring within the intracaldera rocks, and the low-Ti group rocks cropping out in the extracaldera succession.

A similar pattern is observed within the Brennecke Formation of eastern Palmer Land (Wever & Storey, 1992), which is also characterized by low- and high-TiO_2 rocks (high-Ti: >0·65 wt % TiO_2; low-Ti: <0·5 wt % TiO_2).

Trace element geochemistry

The Mount Poster Formation rhyolites are characterized by significantly higher mean Nb (~17 ppm) and Zr (~300 ppm) contents than the rhyolites of the Middle Jurassic Mapple Formation (Nb ~10 ppm; Zr ~180 ppm). Trace element variation within the high-Ti group is evident in several trace element diagrams (e.g. Eu/Eu* vs Sr; Fig. 5a), and is a function of plagioclase fractionation. However, the two rhyolites (R.6892.1, R.7102.1; Table 1) of the low-Ti group have high Sr (~200 ppm) but low Eu/Eu* relative to the high-Ti group, which suggests the two groups are not related by plagioclase fractionation. REE abundances show little variation

Table 1: Selected geochemical and isotopic analyses of Early Jurassic volcanic rocks of the Mount Poster Formation (Antarctic Peninsula)

Sample:	R.6871.3	R.6873.1	R.6874.1	R.6878.1	R.6888.2	R.6889.2	R.7111.1	R.6893.1	R.7103.1	R.7108.2	R.7102.1	R.6892.1
Location:	Wasilew.	Sky-Hi	Sky-Hi	Sky-Hi	Ballard	Ballard	Jenkins	Ballard	Jenkins	Potter	Jenkins	Ballard
Group:	High-Ti	High-Ti	High-Ti	High-Ti	High-Ti	High-Ti	High-Ti	High-Ti	High-Ti	High-Ti	Low-Ti	Low-Ti
SiO_2	72·06	69·45	67·47	70·41	69·62	69·17	70·69	69·68	70·94	72·09	75·02	75·92
TiO_2	0·84	0·78	0·77	0·75	0·78	0·73	0·72	0·74	0·73	0·76	0·4	0·29
Al_2O_3	11·75	13·15	13·01	12·94	13·32	13·30	13·01	13·59	13·01	12·53	12·43	10·36
Fe_2O_3*	4·52	5·44	4·78	5·06	4·87	4·99	4·77	4·86	4·87	4·28	3·09	3·44
MnO	0·07	0·08	0·09	0·09	0·07	0·07	0·07	0·06	0·06	0·06	0·04	0·02
MgO	1·51	1·46	1·28	1·67	1·47	1·34	1·10	1·25	1·20	1·43	0·71	0·36
CaO	1·32	1·65	1·99	1·42	2·31	2·45	2·29	2·34	2·31	1·37	1·84	7·48
Na_2O	2·95	2·15	1·64	2·05	1·58	1·76	1·75	2·22	1·98	2·39	1·10	0·00
K_2O	3·67	4·13	4·49	5·00	4·41	4·29	4·54	4·16	4·26	3·09	4·00	1·18
P_2O_5	0·24	0·20	0·21	0·20	0·20	0·20	0·18	0·22	0·20	0·19	0·04	0·03
LOI	1·17	1·71	3·88	0·77	1·67	1·51	1·24	1·27	0·63	1·74	1·17	1·09
Total	100·10	100·18	99·59	100·35	100·29	99·81	100·36	100·38	100·18	99·92	99·85	100·17
Trace elements by XRF												
Cr	31	29	36	28	33	42	25	25	27	31	28	21
Cu	6	18	6	17	15	15	15	15	13	9	11	8
Ga	12	21	19	18	18	20	16	17	17	15	17	19
Nb	16	18	16	16	16	17	15	15	14	15	15	15
Ni	13	15	15	16	16	16	14	16	16	13	9	12
Rb	92·5	175·0	214·6	200·2	165·8	187·0	182·3	165·0	179·5	167·1	203·1	58·1
Sr	66	128	141	130	150	124	149	150	155	79	198	200
V	54	87	80	78	78	79	69	69	69	75	24	42
Y	47	50	49	48	47	45	43	48	43	47	34	37
Zn	69	59	61	88	83	73	68	75	63	69	66	33
Zr	284	337	297	328	292	292	264	286	260	267	244	228
Trace elements by ICP-MS												
Pb	18·6	19·5	13·9	25·1	18·4	22·9	26·1	27·7	28·3	9·0	22·8	20·5
Ba	757	741	943	875	864	845	838	882	803	675	879	113
Hf	6·8	8·8	7·3	8·0	7·6	7·5	6·5	7·1	6·3	6·5	6·6	6·1
Th	16·2	19·4	18·2	18·6	17·7	17·5	16·1	17·3	16·4	17·6	14·9	12·8
Ta	1·12	1·25	1·22	1·36	1·22	1·23	1·18	1·15	1·05	1·18	1·12	1·12
U	2·88	4·18	3·81	3·58	3·64	3·48	3·43	3·52	2·80	3·75	3·89	2·94
Cs	1·4	6·1	6·4	8·3	5·1	5·4	6·6	4·9	7·8	6·3	16·4	1·7
La	42·1	44·5	48·6	45·6	47·8	42·7	41·4	44·2	37·5	37·8	40·1	27·9
Ce	94·3	104·3	103·1	97·6	98·6	92·5	89·8	96·5	83·7	81·6	85·5	65·7
Pr	12·2	12·7	12·9	12·0	12·4	11·3	11·1	11·9	10·7	10·4	10·4	8·1
Nd	49·9	51·2	52·3	48·9	49·3	45·3	44·1	48·4	43·7	42·7	40·5	33·0
Sm	9·9	10·1	10·2	9·6	9·5	9·1	8·5	9·7	8·7	8·7	7·4	6·5
Eu	1·49	1·65	1·66	1·58	1·66	1·52	1·47	1·66	1·46	1·35	1·03	0·84
Gd	9·3	9·5	9·5	9·1	9·0	8·6	8·1	9·4	8·3	8·3	6·5	6·3
Tb	1·35	1·42	1·38	1·36	1·34	1·27	1·20	1·36	1·23	1·31	0·98	0·98
Dy	8·00	8·27	8·22	7·87	7·98	7·53	7·14	8·05	7·31	7·61	5·78	6·07
Ho	1·64	1·75	1·65	1·65	1·63	1·57	1·47	1·65	1·49	1·60	1·19	1·28
Er	4·41	4·72	4·48	4·51	4·41	4·20	4·07	4·44	4·14	4·42	3·33	3·69
Tm	0·66	0·68	0·65	0·68	0·66	0·65	0·58	0·65	0·59	0·64	0·51	0·55
Yb	4·2	4·5	4·1	4·5	4·2	4·1	3·9	4·2	3·9	4·2	3·4	3·6
Lu	0·64	0·71	0·64	0·70	0·66	0·64	0·61	0·64	0·60	0·65	0·51	0·61
$^{87}Sr/^{86}Sr_{(m)}$	0·731232		0·730260		0·729256	0·730457	0·730546	0·728836	0·728102	0·735058	0·723727	0·712878
$^{87}Sr/^{86}Sr_{(185)}$	0·71965		0·71829		0·72056	0·71866	0·72057	0·72021	0·71885	0·71799	0·71560	0·71062
$^{147}Sm/^{144}Nd$	0·1229		0·1198		0·1221	0·1238	0·1212	0·1219	0·1268	0·1274	0·1156	0·1253
$^{143}Nd/^{144}Nd_{(m)}$	0·512160		0·512173		0·512162	0·512166	0·512146	0·512151	0·512198	0·512170	0·512299	0·512430
$^{143}Nd/^{144}Nd_{(185)}$	0·512025		0·512041		0·512014	0·512016	0·511999	0·512003	0·512044	0·512030	0·512172	0·512278
$\varepsilon Nd_{(185)}$	−7·7		−7·4		−7·5	−7·5	−7·8	−7·7	−6·9	−7·6	−4·9	−2·4
T_{DM}	1612		1590		1574	1571	1594	1589	1532	1605	1406	1189

*Total Fe reported as Fe_2O_3.
Major elements given in wt % and trace elements in ppm. Methods are reported in the text. Location: Wasilew., Mount Wasilewski (75°10′S, 071°23′W); Sky-Hi, Sky-Hi Nunataks (74°54′S, 071°30′W); Ballard, Mount Ballard (75°10′S, 070°00′W); Jenkins, Mount Jenkins (75°08′S, 069°11′W); Potter, Potter Peak (75°09′S, 068°49′W).

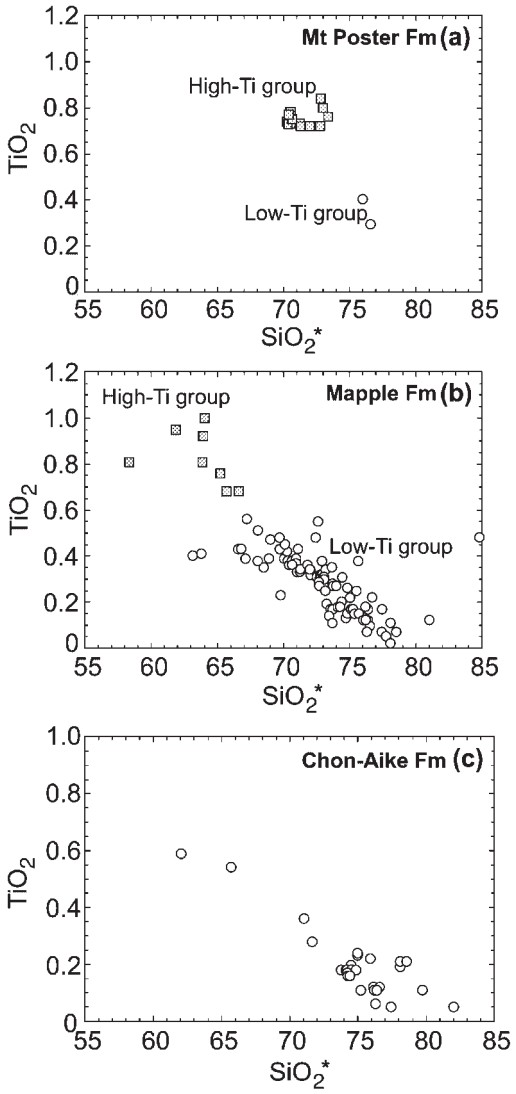

Fig. 4. TiO_2 vs SiO_2 plots for volcanic rocks from (a) Mount Poster Formation, (b) Mapple Formation and (c) Chon Aike Formation (Pankhurst *et al.*, 1998). SiO_2 is calculated to volatile-free totals of 100% (SiO_2*).

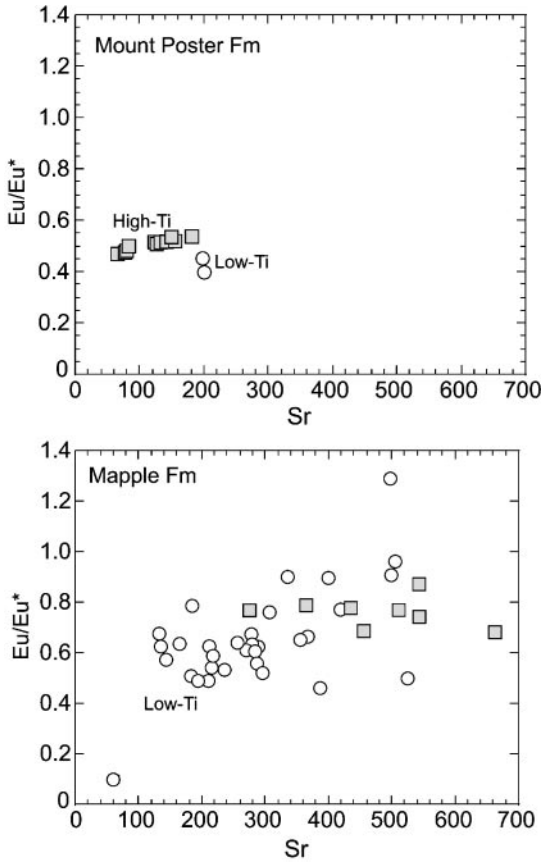

Fig. 5. Eu/Eu* vs Sr plots for volcanic rocks from (a) Mount Poster Formation and (b) Mapple Formation, illustrating the strong control of plagioclase fractionation.

throughout the Mount Poster Formation (Fig. 6a). The high-Ti group exhibit light REE (LREE) enrichment (La_N/Lu_N = 6·0–7·8), moderate negative Eu anomalies (Eu/Eu* = 0·47–0·54) and flat middle REE (MREE) to heavy REE (HREE) abundances, whereas the low-Ti rhyolites have more variable LREE enrichment (La_N/Lu_N = 4·7–8·1) and more pronounced negative Eu anomalies (Eu/Eu* = 0·40–0·45).

Multi-element plots for the Mount Poster Formation are shown in Fig. 7a (normalized to primitive mantle; Sun & McDonough, 1989). A clear difference between the high- and low-Ti groups is illustrated, with the low-Ti group characterized by pronounced relative depletions in almost all elements, with the exception of Sr, although discrepancies occur in the more mobile elements (Rb, Ba, K), which probably reflect low-temperature alteration. The majority of samples fall within the high-Ti group and exhibit fairly homogeneous trace element abundances, which are characteristic of arc magmas (Pearce, 1982). Negative anomalies in Sr, P and Ti are consistent with extensive fractional crystallization of plagioclase, apatite and Fe–Ti oxides, respectively.

Only limited trace element data are available for silicic rocks from the Brennecke Formation (Wever & Storey, 1992). REE patterns are very similar to those of the Mount Poster Formation, with Ce_N/Yb_N ratios between four and six and a negative Eu anomaly of Eu/Eu* ~0·4, and also very similar multi-element distributions (Fig. 7b; Wever & Storey, 1992; unpublished data, 1998).

Sr and Nd isotope geochemistry

Ten rhyolite samples from the Mount Poster Formation have been analysed for Sr and Nd isotope ratios (Table 1). Ratios have been corrected to initial values using an

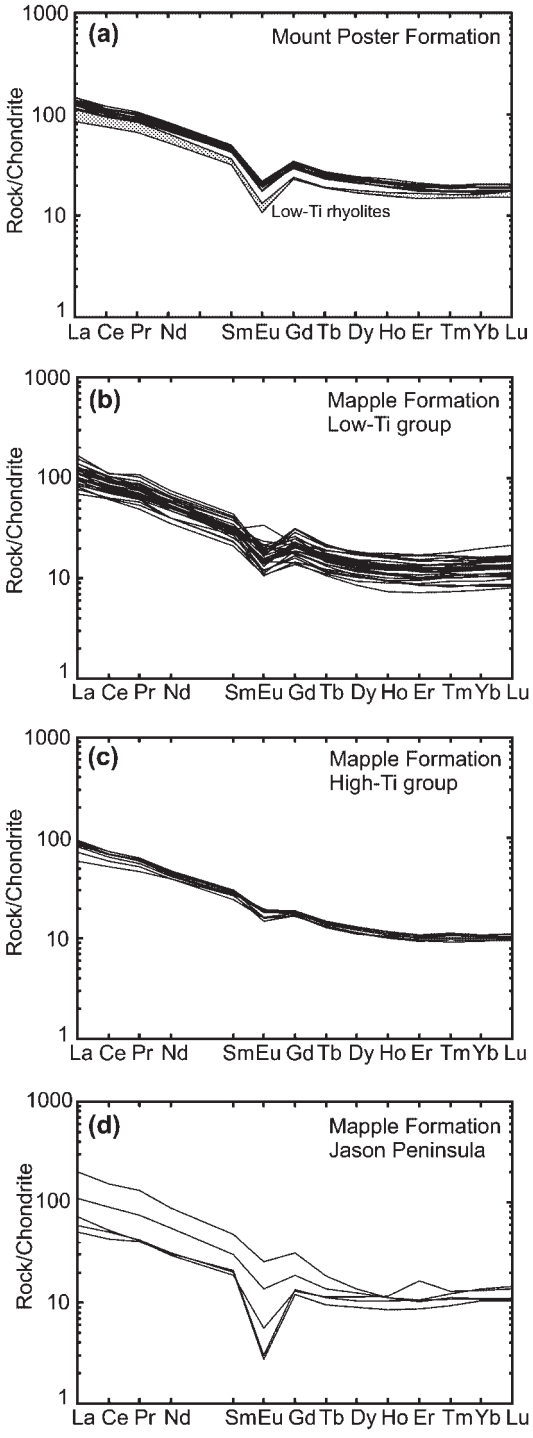

Fig. 6. Chondrite-normalized (Nakamura, 1974) REE diagrams for volcanic rocks from the (a) Mount Poster Formation, (b) Mapple Formation (low-Ti), (c) Mapple Formation (high-Ti) and (d) Mapple Formation (Jason Peninsula).

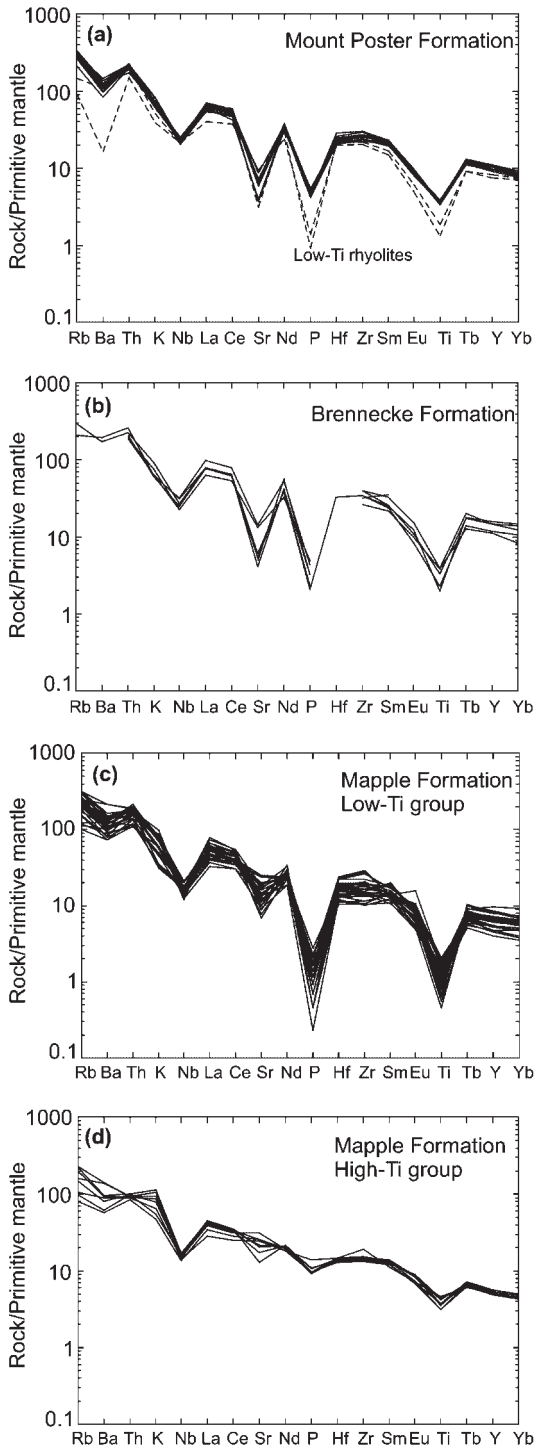

Fig. 7. Primitive mantle normalized (Sun & McDonough, 1989) plots for volcanic rocks from (a) Mount Poster Formation (high- and low-Ti groups), (b) Brennecke Formation (Wever & Storey, 1992; unpublished data, 1998), (c) Mapple Formation (low-Ti) and (d) Mapple Formation (high-Ti).

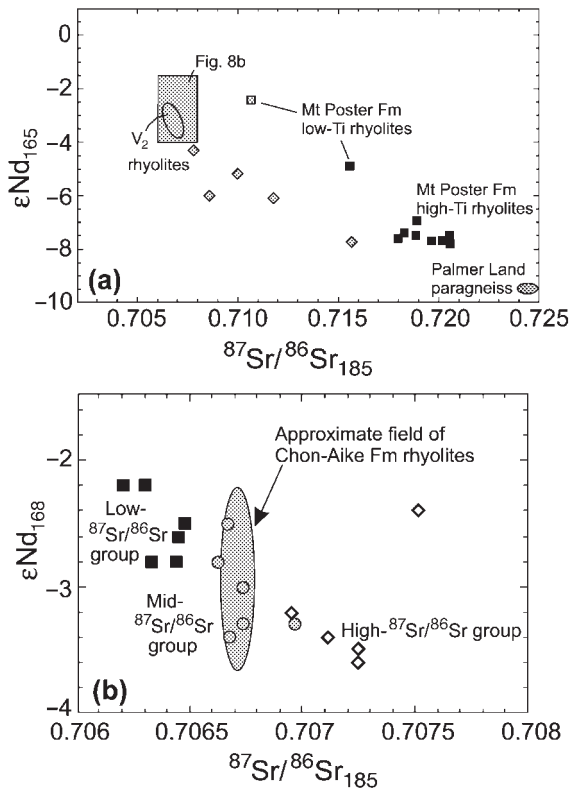

Fig. 8. εNd_i vs $^{87}Sr/^{86}Sr_i$ plots for volcanic rocks from (a) Mount Poster (this study) and Brennecke (Wever & Storey, 1992; I. L. Millar, unpublished data, 1998) formations. Palmer Land paragneiss data are from Wever *et al.* (1994). (b) Mapple Formation high-, mid- and low-$^{87}Sr/^{86}Sr_{168}$ subgroups. Field for Chon Aike Formation rhyolites is from Pankhurst & Rapela (1995).

eruption age of 185 Ma, corresponding to the V_1 event. The $^{87}Sr/^{86}Sr_{185}$ ratios of the Mount Poster Formation are considerably more radiogenic than the rhyolites of the Middle Jurassic Mapple Formation (next section). The samples cover a wide range in $^{87}Sr/^{86}Sr_{185}$ (0·7106–0·7206), and a range in εNd_{185} from −2·4 to −7·8 (Fig. 8a). The high-Ti group cluster in both $^{87}Sr/^{86}Sr_{185}$ (0·7180–0·7206) and εNd_{185} (−6·9 to −7·8), whereas the low-Ti group are characterized by less radiogenic $^{87}Sr/^{86}Sr_{185}$ (0·7106–0·7156) and less negative εNd_{185} (−2·4 to −4·9).

Rhyolitic and dacitic volcanic rocks from the nearby Brennecke Formation of eastern Palmer Land (Wever & Storey, 1992) have comparable εNd_{185} (−4·3 to −7·7) and similar $^{87}Sr/^{86}Sr_{185}$ (0·7078–0·7157; I. L. Millar, unpublished data, 1998) to the roughly contemporaneous Mount Poster Formation (Fig. 8a). The Brennecke Formation also shows very similar characteristics in terms of SiO_2 and $^{87}Sr/^{86}Sr_{185}$ to the Mount Poster Formation. The high-Ti rocks (>0·65% TiO_2) of the Brennecke Formation are characterized by more radiogenic $^{87}Sr/^{86}Sr_{185}$ (0·7100–0·7157) and εNd_{185} (−5·2 to −7·7) than the lower-Ti (>0·5% TiO_2) rocks, which have $^{87}Sr/^{86}Sr_{185}$ of 0·7078–0·7086 and εNd_{185} of −4·3 to −6·0.

Middle Jurassic volcanic rocks (V_2) of the Mapple Formation

Major element geochemistry

The SiO_2–TiO_2 (Fig. 4b) plot clearly illustrates that two groups can also be recognized within the Mapple Formation: a high-Ti group (0·68–1·00 wt % TiO_2), characterized by intermediate compositions (~62–67 wt % SiO_2), and a low-Ti group (0·02–0·56 wt % TiO_2), dominated by dacites and rhyolites (~64–77 wt % SiO_2). Selected analyses from the Mapple Formation are given in Table 2 (a full dataset for the Mapple Formation is available on the *Journal of Petrology* Web site at http://www.petrology.oupjournals.org), and differences between the low- and high-Ti groups are defined in Table 3.

The Chon Aike Formation is also dominated by low-Ti compositions, with only one sample plotting within the high-Ti group (Fig. 4c).

Trace element geochemistry

As well as the contrast in TiO_2 concentrations between the high- and low-Ti groups, there are key differences in Sr, Th and Y (Table 3). Trace element variation within the Mapple Formation, evident on several trace element diagrams (e.g. Eu/Eu* vs Sr; Fig. 5b), is a function of plagioclase-dominated fractionation. Rare earth element (REE) abundances are fairly homogeneous throughout the low-Ti group of the Mapple Formation (Fig. 6b). They all exhibit LREE enrichment (La_N/Lu_N = 4·0–16·9), and pronounced negative Eu anomalies (Eu/Eu* ~0·65; range 0·46–0·98). An exception is sample R.6629·5, which has a positive Eu anomaly (Eu/Eu* = 1·29). All samples have convex-down MREE to HREE patterns, with slightly concave-up HREE patterns. REE patterns for the high-Ti group are flatter (Fig. 6c), with small negative Eu anomalies (Eu/Eu* = 0·68–0·87) and less pronounced LREE enrichment (La_N/Lu_N = 5·9–8·8). REE abundances from Jason Peninsula rhyolites (Fig. 6d) are more varied than those for rhyolites from the Cape Disappointment area. They are characterized by more pronounced negative Eu anomalies (Eu/Eu* = 0·17–0·65) and a broad range in LREE enrichment (La_N/Lu_N = 3·4–18·2), which may reflect their extreme alteration.

The high-Ti group is characterized by increasing normalized abundances as element incompatibility increases towards the left of Fig. 7c. Rb, Ba and Th are significantly enriched relative to Nb and the LREE, a feature of magmas formed in magmatic arcs (Pearce, 1982; Thompson *et al.*, 1984). The depletions in Nb and Ti relative to

Table 2: Selected geochemical and isotopic analyses of Middle Jurassic volcanic rocks of the Mapple Formation (Antarctic Peninsula)

Sample:	R.6622.4	R.6623.3	R.6608.2	R.6863.3	R.6605.4	R.6605.6	R.6607.3	R.6609.3	R.6610.3	R.6612.4	R.6614.2	R.6618.1
Glacier:	Stubb	Stubb	Pequod	Pequod	Pequod	Pequod	Pequod	Pequod	Pequod	Rachel	Pequod	Rachel
Group:	High-Ti	High-Ti	High-Ti	High-Ti	Low-Ti	Low-Ti	Low-Ti	Low-Ti	Low-Ti	Low-Ti	Low-Ti	Low-Ti
$^{87}Sr/^{86}Sr$ subgroup:		mid	mid			mid	mid	high	mid	low	low	high
SiO_2	62·88	60·6	63·35	62·85	72·35	74·95	72·04	74·76	75·35	74·45	72·25	77·22
TiO_2	0·92	0·95	0·68	0·76	0·14	0·18	0·29	0·15	0·17	0·17	0·27	0·08
Al_2O_3	16·28	16·07	14·94	15·87	15·28	13·88	14·19	12·81	12·27	13·07	14·28	11·89
Fe_2O_3*	6·03	6·94	4·84	5·51	1·92	1·42	2·40	2·26	1·59	1·70	2·40	1·24
MnO	0·10	0·11	0·10	0·10	0·03	0·03	0·04	0·05	0·02	0·04	0·03	0·01
MgO	2·34	2·54	1·56	2·23	0·34	0·24	0·43	0·06	0·16	0·40	0·41	0·00
CaO	3·67	4·86	3·86	3·15	0·61	0·97	1·61	0·73	0·96	1·10	1·81	0·53
Na_2O	4·33	3·72	3·16	2·27	3·42	2·13	3·15	3·56	2·24	4·33	3·00	3·34
K_2O	1·66	1·95	2·39	3·39	4·40	4·54	4·91	4·75	5·88	3·82	4·82	4·79
P_2O_5	0·21	0·20	0·21	0·23	0·02	0·03	0·08	0·03	0·03	0·06	0·08	0·02
LOI	1·74	1·80	4·38	4·12	1·51	1·21	0·88	0·47	1·34	0·53	0·68	0·51
Total	100·15	99·74	99·46	100·48	100·01	99·57	100·03	99·63	100·01	99·67	100·04	99·62
Trace elements by XRF												
Cr	15	10	15	18	9	11	13	10	15	12	13	9
Cu	3	7	10	11	1	1	4	6	1	5	6	2
Ga	15	18	19	19	19	20	18	15	13	10	16	19
Nb	9	9	10	10	11	11	9	12	10	8	9	17
Ni	3	3	3	7	0	0	2	2	1	3	3	3
Rb	61	69	94	141	186	203	150	133	201	105	133	431
Sr	409	540	458	271	204	389	245	215	143	123	295	15
V	167	185	112	111	10	15	34	6	5	18	29	8
Y	23	23	22	24	37	39	23	28	27	21	22	90
Zn	78	81	78	84	59	59	43	78	46	27	38	17
Zr	199	182	156	165	156	175	155	203	211	108	138	101
Trace elements by ICP-MS												
Pb	9·9	10·2	11·2	8·2	19·5	26·5	18·1	27†	23·8	8·7	16·3	31†
Ba	420	651	558	731	833	1390	955	1089†	1096	728	912	
Hf	4·6	4·3	4·3	4·4	5·3	5·5	3·5		5·6	3·0	4·0	
Th	8·5	7·5	8·3	8·7	18·5	16·2	15·3	16†	14·9	17·1	15·0	-
Ta	0·75	0·70	0·77	0·81	1·10	0·96	0·63		0·93	0·95	0·67	
U	2·01	1·78	2·12	2·05	3·77	3·53	2·22		3·37	3·06	2·17	
Cs	1·6	0·8	5·4	5·1	6·9	3·5	1·4		2·9	0·5	1·9	
La	30·7	28·9	29·1	29·8	54·2	50·7	41·9		42·5	26·8	38·6	
Ce	63·1	59·2	60·2	62·8	95·1	96·7	89·9		79·3	52·5	82·9	
Pr	7·6	7·1	7·4	7·7	13·0	12·3	10·3		9·7	6·0	9·8	
Nd	28·6	26·8	28·1	29·5	46·5	43·9	39·5		33·9	22·2	36·6	
Sm	5·9	5·6	5·9	6·2	8·9	8·4	6·2		6·3	4·3	5·9	
Eu	1·39	1·49	1·24	1·44	1·41	1·27	1·14		1·14	0·83	0·92	
Gd	4·9	4·7	4·9	5·1	8·7	8·4	5·0		5·8	3·8	4·7	
Tb	0·74	0·68	0·72	0·75	1·13	1·09	0·69		0·77	0·57	0·62	
Dy	4·17	3·86	4·18	4·30	6·06	6·11	3·65		4·40	3·19	3·57	
Ho	0·82	0·76	0·83	0·86	1·23	1·25	0·72		0·92	0·69	0·71	
Er	2·30	2·12	2·27	2·39	3·44	3·48	1·97		2·76	2·00	1·91	
Tm	0·36	0·33	0·34	0·37	0·50	0·55	0·28		0·41	0·32	0·29	
Yb	2·3	2·1	2·2	2·3	3·3	3·4	1·9		2·7	2·1	1·8	
Lu	0·36	0·34	0·34	0·35	0·52	0·54	0·30		0·44	0·34	0·28	
$\delta^{18}O_{quartz}$(‰)												
$^{87}Sr/^{86}Sr_{(m)}$	0·707703	0·707541			0·712879	0·710374	0·711747	0·710725	0·715981	0·711500	0·710659	
$^{87}Sr/^{86}Sr_{(168)}$	0·70667	0·70666			0·70656	0·70674	0·70751	0·70645	0·70618	0·70559	0·70755	
$^{147}Sm/^{144}Nd$	0·1164	0·1180				0·1114	0·1015	0·1163		0·1187		0·1621
$^{143}Nd/^{144}Nd_{(m)}$	0·512421	0·512418				0·512393	0·512413	0·512414		0·512437		0·512457
$^{143}Nd/^{144}Nd_{(168)}$	0·512293	0·512288				0·512271	0·512301	0·512286		0·512306		0·512279
$\varepsilon Nd_{(168)}$	−2·5	−2·6				−3·0	−2·4	−2·6		−2·3		−2·8
T_{DM}	1188	1195				1223	1214	1199		1167		1210

Sample:	R.6618.7	R.6619.3	R.6621.2	R.6624.1	R.6625.2	R.6625.3	R.6626.1	R.6627.3	R.6627.6	R.6627.7	R.6628.3	R.6629.4
Glacier:	Rachel	Rachel	Stubb	Stubb	Stubb	Stubb	Stubb	Stubb	Stubb	Stubb	Stubb	Stubb
Group:	Low-Ti	Low-Ti	Low-Ti	Low-Ti	Low-Ti	Low-Ti	Low-Ti	Low-Ti	Low-Ti	Low-Ti	Low-Ti	Low-Ti
$^{87}Sr/^{86}Sr$ subgroup:	low	low	low	low	mid	low	low	low	mid	low	mid	low
SiO_2	73·90	66·50	72·28	71·65	74·36	69·80	68·31	73·79	67·77	74·53	71·17	74·17
TiO_2	0·20	0·43	0·25	0·19	0·15	0·43	0·23	0·18	0·35	0·12	0·34	0·22
Al_2O_3	13·43	16·29	13·75	13·72	13·59	15·23	15·39	13·60	15·59	13·17	15·81	13·43
Fe_2O_3*	1·99	4·63	2·31	2·23	1·68	2·96	2·56	1·99	3·85	1·76	2·95	2·62
MnO	0·05	0·10	0·05	0·06	0·03	0·01	0·06	0·05	0·06	0·04	0·04	0·05
MgO	0·38	0·92	0·48	0·28	0·03	0·45	0·27	0·17	0·79	0·21	0·59	0·29
CaO	1·38	4·62	1·90	1·96	0·96	1·98	1·86	1·46	3·24	1·11	2·41	1·53
Na_2O	3·33	3·51	3·20	4·07	3·58	3·22	4·16	3·85	3·84	1·89	3·41	4·58
K_2O	4·63	2·80	4·49	3·62	4·95	3·96	5·02	4·46	3·35	5·19	2·08	1·94
P_2O_5	0·05	0·10	0·08	0·04	0·02	0·09	0·05	0·03	0·09	0·02	0·07	0·04
LOI	0·57	0·56	0·71	2·24	0·56	2·18	2·39	0·81	1·37	1·97	1·02	0·65
Total	99·90	100·47	99·50	100·06	99·91	100·32	100·29	100·38	100·30	100·00	99·89	99·51
Trace elements by XRF												
Cr	8	12	11	8	9	19	9	8	10	18	15	8
Cu	1	5	4	1	2	2	0	1	4	1	5	0
Ga	16	20	16	17	19	17	19	16	19	18	20	16
Nb	9	8	9	11	13	10	13	12	10	11	9	10
Ni	2	2	5	1	0	4	0	1	2	0	4	0
Rb	175	80	167	140	189	142	161	166	128	203	98	75
Sr	282	496	269	246	177	446	340	223	392	167	510	276
V	14	85	23	5	6	60	8	7	56	10	39	17
Y	21	24	25	31	36	26	34	33	27	31	30	28
Zn	53	78	38	57	57	43	58	55	69	56	52	50
Zr	140	187	123	181	231	223	191	167	210	157	152	221
Trace elements by ICP-MS												
Pb	25·5	16·0	23·1	20·1	28·0	16†	32·2	20·4	18·3	27·7	28·9	18·7
Ba	708	808	637	766	896	1378†	958	816	678	967	598	720
Hf	4·4	5·4	3·3	5·4	6·8		6·0	4·2	5·6	4·7	4·8	5·9
Th	13·1	9·8	13·8	14·3	16·9	9†	16·5	13·9	13·2	11·8	15·8	11·6
Ta	0·91	0·90	1·07	0·95	1·13		1·33	0·94	0·71	0·94	1·04	0·90
U	2·97	2·27	3·24	3·26	3·66		2·66	3·29	2·94	2·96	4·78	2·55
Cs	10·4	3·3	1·9	4·2	2·7		5·1	3·1	2·4	4·8	7·3	4·8
La	31·3	27·8	22·7	33·0	45·3		36·8	31·9	31·9	32·6	35·9	38·9
Ce	61·6	61·07	53·6	67·5	90·0		79·8	69·2	66·9	69·6	73·3	79·0
Pr	7·4	7·4	6·5	8·1	11·3		9·5	8·3	7·9	8·4	9·0	10·0
Nd	25·2	29·8	24·9	32·5	41·0		37·6	33·0	31·9	29·7	32·6	36·0
Sm	4·7	5·6	4·8	6·5	8·0		7·7	6·6	6·1	5·8	6·4	7·0
Eu	0·94	1·67	0·82	1·30	1·33		1·57	1·09	1·49	1·21	1·03	1·39
Gd	4·4	4·8	4·0	5·8	7·9		6·8	5·8	5·5	5·9	6·2	6·4
Tb	0·60	0·71	0·64	0·90	1·08		1·00	0·87	0·82	0·80	0·87	0·87
Dy	3·51	4·12	3·77	5·21	6·27		5·85	5·26	4·73	4·59	5·01	4·81
Ho	0·72	0·82	0·77	1·04	1·27		1·20	1·13	0·95	0·94	1·01	0·98
Er	2·16	2·28	2·24	3·03	3·76		3·33	3·09	2·64	2·73	2·88	2·88
Tm	0·35	0·34	0·36	0·48	0·57		0·51	0·46	0·40	0·42	0·43	0·43
Yb	2·3	2·3	2·5	3·2	3·6		3·6	3·2	2·7	2·7	2·8	2·9
Lu	0·35	0·38	0·4	0·52	0·54		0·58	0·51	0·44	0·42	0·42	0·45
$\delta^{18}O_{quartz}$ (‰)	6·4	7·4						9·5			8·2	
$^{87}Sr/^{86}Sr_{(m)}$	0·710491	0·707575	0·710657	0·710263	0·714070	0·708535	0·709689	0·711403	0·709038	0·714558	0·708296	0·708320
$^{87}Sr/^{86}Sr_{(168)}$	0·70621	0·70646	0·70641	0·70632	0·70674	0·70633	0·70644	0·70630	0·70680	0·70618	0·70697	0·70649
$^{147}Sm/^{144}Nd$	0·1117				0·1179	0·1192		0·1223			0·1174	
$^{143}Nd/^{144}Nd_{(m)}$	0·512432				0·512380	0·512411		0·512444			0·512382	
$^{143}Nd/^{144}Nd_{(168)}$	0·512309				0·512250	0·512280		0·512310			0·512253	
$\varepsilon Nd_{(168)}$	−2·2				−3·3	−2·8		−2·2			−3·3	
T_{DM}	1163				1253	1208		1162			1249	

Table 2: continued

Sample:	R.6629.5	R.6630.2	R.6630.3	R.6630.4	R.6631.2	R.6632.2	R.6632.3	R.6632.7	R.6634.5	R.6851.3	R.6861.1	R.6911.3
Glacier:	Stubb	Stubb	Stubb	Stubb	Stubb	Stubb	Stubb	Stubb	Stubb	Mapple	Mapple	Mapple
Group:	Low-Ti	Low-Ti	Low-Ti	Low-Ti	Low-Ti	Low-Ti	Low-Ti	Low-Ti	Low-Ti	Low-Ti	Low-Ti	Low-Ti
$^{87}Sr/^{86}Sr$ subgroup:	mid	mid	low	low	mid	low	low	mid	low	high	high	high
SiO_2	70·09	74·16	68·69	75·63	72·01	74·36	76·19	69·45	76·08	68·49	70·27	72·91
TiO_2	0·37	0·25	0·42	0·12	0·38	0·26	0·12	0·45	0·10	0·43	0·33	0·27
Al_2O_3	14·79	13·34	14·59	13·07	13·97	13·20	13·06	15·06	12·63	15·05	14·43	13·62
Fe_2O_3*	3·10	2·82	4·38	1·55	2·93	2·34	1·12	3·34	1·21	3·52	3·30	2·66
MnO	0·08	0·05	0·07	0·06	0·07	0·04	0·03	0·08	0·02	0·05	0·06	0·05
MgO	0·55	0·33	0·70	0·09	0·63	0·51	0·11	0·72	0·07	0·98	1·00	0·50
CaO	3·30	1·06	2·65	1·03	2·64	2·51	0·87	3·32	1·00	1·19	1·18	0·79
Na_2O	3·61	3·40	2·62	3·21	3·96	4·24	3·97	3·62	3·63	2·65	3·89	4·80
K_2O	2·82	2·71	3·52	4·63	2·14	1·89	4·24	2·98	4·68	5·75	4·42	3·16
P_2O_5	0·07	0·04	0·12	0·02	0·06	0·05	0·02	0·09	0·01	0·11	0·11	0·07
LOI	0·82	1·33	2·37	0·73	0·80	0·71	0·54	0·62	0·41	1·64	1·11	0·98
Total	99·60	99·51	100·13	100·15	99·59	100·09	100·27	99·71	99·84	99·84	100·10	99·81
Trace elements by XRF												
Cr	12	9	14	14	8	9	9	9	9	17	16	16
Cu	7	1	7	4	1	2	0	3	0	9	5	3
Ga	21	18	18	16	18	16	16	18	15	17	17	13
Nb	12	12	10	10	11	10	10	12	9	10	10	5
Ni	2	1	4	2	1	4	2	3	1	4	3	2
Rb	103	110	138	144	77	66	121	130	132	175	156	100
Sr	499	269	354	217	493	353	234	422	190	139	203	126
V	12	3	38	6	22	23	7	21	6	62	47	32
Y	42	29	24	29	23	28	28	26	30	25	27	18
Zn	50	54	65	46	63	37	26	58	25	58	57	24
Zr	305	268	202	133	271	165	124	311	103	174	134	133
Trace elements by ICP-MS												
Pb	19·8	19·5	13·9	29·2	26·5	13·9	28·2	20·1	26·5	18†	6†	13·8
Ba	504	788	624	981	613	502	981	643	757	1020†	731†	586
Hf	6·9	6·9	4·9	3·5	7·3	5·0	4·1	7·3	3·7			4·1
Th	9·5	12·1	9·3	16·1	10·0	11·4	16·0	10·1	16·2	15†	15†	14·1
Ta	0·79	0·93	0·76	0·92	0·83	0·83	1·01	0·80	1·10			1·10
U	3·67	2·67	2·13	3·54	2·55	3·56	3·25	2·40	3·82			2·50
Cs	2·3	3·1	12·0	2·3	1·7	4·7	1·8	10·5	1·3			1·0
La	28·6	40·7	27·5	36·3	33·5	41·6	39·3	37·0	25·6			36·9
Ce	65·2	82·1	61·5	78·1	68·0	82·8	77·2	63·8	54·0			75·7
Pr	8·0	10·6	7·7	9·2	8·6	10·2	9·5	7·7	7·0			8·7
Nd	32·3	39·4	31·8	35·6	32·0	35·6	32·7	31·0	25·3			32·6
Sm	6·2	7·6	5·7	6·4	6·2	6·6	6·1	6·0	5·5			5·6
Eu	2·62	1·65	1·57	1·07	1·81	1·47	1·09	1·64	0·86			1·14
Gd	6·2	7·2	4·8	5·5	5·9	6·9	6·4	5·0	5·1			4·5
Tb	0·97	0·93	0·71	0·84	0·75	0·85	0·83	0·72	0·84			0·65
Dy	6·15	5·26	3·97	4·81	4·32	4·69	4·61	4·07	4·91			3·56
Ho	1·34	1·03	0·82	0·99	0·86	1·00	0·96	0·85	1·01			0·73
Er	3·87	2·86	2·25	2·83	2·45	2·72	2·75	2·32	3·01			1·97
Tm	0·62	0·43	0·34	0·43	0·38	0·44	0·44	0·37	0·47			0·32
Yb	4·4	2·7	2·3	2·9	2·3	2·7	2·9	2·5	3·0			2·1
Lu	0·74	0·44	0·37	0·47	0·36	0·41	0·45	0·39	0·47			0·34
$\delta^{18}O_{quartz}$ (‰)						7·7		6·1		10·2	10·6	
$^{87}Sr/^{86}Sr_{(m)}$	0·708046	0·709422	0·709191	0·711071	0·707692	0·707685	0·709948	0·708792	0·711283	0·715952	0·712429	0·712328
$^{87}Sr/^{86}Sr_{(168)}$	0·70663	0·70665	0·70652	0·70648	0·70665	0·70644	0·70645	0·70668	0·70648	0·70724	0·70712	0·70695
$^{147}Sm/^{144}Nd$	0·1189			0·1131		0·1089		0·1149		0·1095	0·1100	
$^{143}Nd/^{144}Nd_{(m)}$	0·512385			0·512392		0·512396		0·512373		0·512361	0·512370	
$^{143}Nd/^{144}Nd_{(168)}$	0·512254			0·512268		0·512276		0·512247		0·512241	0·512249	
$\varepsilon Nd_{(168)}$	−3·3			−3·0		−2·8		−3·4		−3·5	−3·4	
T_{DM}	1247			1227		1214		1259		1268	1255	

*Total Fe reported as Fe_2O_3.
†Analysis by XRF.
Major elements given in wt % and trace elements in ppm. Methods are reported in the text. A full dataset for the Mapple Formation is available on the *Journal of Petrology* Web site at http:// www.petrology.oupjournals.org.

Table 3: Geochemical characteristics of the high- and low-Ti groups of the Mapple Formation (Antarctic Peninsula)

	Low-Ti group range (r.m.s.)	High-Ti group range (r.m.s.)
SiO_2	64–78 (72)	57–63 (62)
TiO_2	0·02–0·56 (0·31)	0·68–1·00 (0·83)
Nb	4–15 (9)	9·6–12·1 (11·0)
Rb	66–336 (155)	52–147 (105)
Sr	51–563 (270)	275–663 (487)
Th	6·04–25·68 (14·61)	7·24–8·65 (7·99)
Y	3–63 (29)	22·1–25·5 (23·6)
Zr	42–311 (172)	149–214 (167)
Ba	135–2437 (859)	403–988 (695)

the LILE and REE of similar compatibility (e.g. $Ba_N/Nb_N = 5–12$; $Eu_N/Ti_N = 5–13$; normalized to primitive mantle) is also characteristic of continental magmatic arcs (Pearce, 1982), although the Ti depletion may be a result of fractionation of Fe–Ti oxides.

The low-Ti group have similar patterns (Fig. 7d) to the high-Ti group except that there are larger negative Sr, P and Ti anomalies, consistent with more extensive fractional crystallization of plagioclase, apatite and Fe–Ti oxides.

Isotope (Sr, Nd, O) geochemistry

Fifty-five andesite–rhyolite samples from the Mapple Formation have been analysed for Sr isotope ratios, 22 for Nd isotopes and eight for O isotopes (selected analyses shown in Table 2; age corrected to 168 Ma—see Geochronology section). On the basis of $^{87}Sr/^{86}Sr$, εNd and $\delta^{18}O$, subgroups can be identified within the Mapple Formation, alongside the high- and low-Ti groups discussed above. Three subgroups have been identified principally on the basis of $^{87}Sr/^{86}Sr_{168}$ values (high-, mid- and low-$^{87}Sr/^{86}Sr_{168}$ subgroups), which also broadly correlate with εNd (Fig. 8b) and $\delta^{18}O$ values (Table 4). The high-$^{87}Sr/^{86}Sr_{168}$ subgroup is characterized by uniform $^{87}Sr/^{86}Sr_{168}$ (∼0·7070–0·7074), εNd_{168} (−3·4 to −3·6) and $\delta^{18}O$ values (10·2–10·6), and all rocks from this subgroup are within the low-Ti group of the Mapple Formation. The subgroup has a limited geographical extent, with almost all rocks cropping out in the Mapple Glacier region of eastern Graham Land (Fig. 1b). The high-$^{87}Sr/^{86}Sr_{168}$ subgroup is also characterized by a limited SiO_2 range (70–76 wt %) and moderate Zr (<160 ppm) and Sr (<250 ppm) contents (Table 4). A mid-$^{87}Sr/^{86}Sr_{168}$ subgroup is also recognized and has an outcrop area largely restricted to the Stubb, Pequod and Rachel glaciers (Fig. 1b). The subgroup is also characterized by uniform $^{87}Sr/^{86}Sr_{168}$ (∼0·7065–0·7067), εNd_{168} (−2·4 to −34) and $\delta^{18}O$ values (6·0–8·2; two samples) (Table 2). The mid-$^{87}Sr/^{86}Sr_{168}$ subgroup includes rock types from both the low- and high-Ti groups, such that andesites, dacites and rhyolites all have identical $^{87}Sr/^{86}Sr_{168}$ values, suggesting a relationship involving fractionation. A low-$^{87}Sr/^{86}Sr_{168}$ subgroup largely encompasses the remaining (16) samples, which are again characterized by uniform $^{87}Sr/^{86}Sr_{168}$ (∼0·7062–0·7065), εNd_{168} (−2·2 to −2·8) and $\delta^{18}O$ values (6·4–9·5). This subgroup is mostly restricted to the Stubb Glacier region, but also includes samples from the entire outcrop area of the Mapple Formation. Geographically and chemically, the low- and mid-$^{87}Sr/^{86}Sr_{168}$ subgroups are very similar, although the high-$^{87}Sr/^{86}Sr_{168}$ subgroup is rather more distinct, with more enriched $^{87}Sr/^{86}Sr$, more negative εNd isotopes and elevated $\delta^{18}O$ values.

Rhyolitic rocks from the Chon Aike Formation have isotopic characteristics very similar to the mid-$^{87}Sr/^{86}Sr_{168}$ subgroup of the Mapple Formation (Fig. 8b). Pankhurst & Rapela (1995) reported remarkably homogeneous initial $^{87}Sr/^{86}Sr_{168}$ ratios of 0·7067 ± 0·0005 from ∼30 rhyolites from the Chon Aike and neighbouring Middle Jurassic formations, with εNd_{168} showing more variation, with a total range of −1·8 to −3·9.

RHYOLITE PETROGENESIS

Early Jurassic volcanic rocks (V_1)

The silicic volcanic rocks of the Mount Poster and Brennecke formations of the southern Antarctic Peninsula fall within the Early Jurassic, V_1 (∼185 Ma) event of Pankhurst *et al.* (2000), coincident with the Marifil Formation of northern Patagonia.

The Mount Poster and Brennecke formation rhyolites have strongly radiogenic $^{87}Sr/^{86}Sr$ ratios relative to the Middle Jurassic (V_2) rhyolites of the Mapple Formation. The Mount Poster Formation rhyolites have ranges in $^{87}Sr/^{86}Sr_{185}$ of 0·7106–0·7206, and εNd_{185} of −2·4 to −7·8, although rocks from the high-Ti group have a smaller isotopic range ($^{87}Sr/^{86}Sr_{185}$ = 0·7180–0·7206; εNd_{185} = −6·9 to −7·8; Table 1). The high-Ti group of the Mount Poster Formation corresponds to the main intracaldera succession of moderate to strongly welded ignimbrites and rare lava flows. The small isotopic range exhibited for such a large volume of rhyolite suggests residence in a long-lived, convecting magma chamber, to achieve homogenization (see Poitrasson & Pin, 1998), and the caldera-related setting indicates that the magma chamber was situated in the upper crust. The Sr and Nd

Table 4: Definition of $^{87}Sr/^{86}Sr$ subgroups of the Mapple Formation (Antarctic Peninsula) and comparison with the Chon Aike Formation (Patagonia)

	Mapple Formation			Chon Aike Formation
	Low-$^{87}Sr/^{86}Sr$ subgroup	Mid-$^{87}Sr/^{86}Sr$ subgroup	High-$^{87}Sr/^{86}Sr$ subgroup	
Ti group	Low-Ti group	Low- and high-Ti groups	Low-Ti group	Low-Ti group
$^{87}Sr/^{86}Sr_{(168)}$	0·7061–0·7065	0·7065–0·7068	0·7070–0·7076	0·7066–0·7068
$\varepsilon Nd_{(168)}$	−2·2 to −2·8	−2·5 to −3·4	−3·2 to −3·6	−2 to −4
$\delta^{18}O_{quartz}$ (‰)	6·4–9·5	6·1–8·2	10·2–10·6	n.a.
SiO_2 range (wt %)	66–77	60–76	69–75	66–76
Zr range	~120–220	~120–300	~140–170	~80–300
Sr range	~150–440	~200–540	~130–250	~30–250
Field characteristics	Moderate to poorly welded thin ignimbrite units. Interbedded lavas, air-fall and volcaniclastic units	Moderate to poorly welded thin ignimbrite units. Rare mafic dykes and lava flows	Thick sequences of strongly welded ignimbrite. Mafic rocks are absent	Dominated by moderately welded ignimbrites, up to 100 m thick. Rare lavas and epiclastic deposits

isotopic ratios of the Mount Poster Formation volcanic rocks clearly suggest a significant crustal component in their petrogenesis, and the strongly radiogenic $^{87}Sr/^{86}Sr$ ratios and negative εNd values indicate a middle–upper-crustal component.

Silicic volcanic rocks from the Brennecke Formation have a range in $^{87}Sr/^{86}Sr_{185}$ of 0·7078–0·7157 and εNd_{185} of −4·3 to −7·7 (Wever & Storey, 1992; I. L. Millar, unpublished data, 1998). The rhyolite with the least radiogenic $^{87}Sr/^{86}Sr_{185}$ (0·7078) and least negative εNd_{185} (−4·3) indicates lower levels of crustal contamination. The Marifil Formation rhyolites have $^{87}Sr/^{86}Sr_i$ ratios of ~0·7065–0·7070 and εNd_i values of ~−4 to −6 (Pankhurst & Rapela, 1995). These values are comparable with the 'least contaminated' composition from the Brennecke Formation and also fall within the range of the V_2 rhyolites from the Mapple and Chon Aike formations.

Pankhurst & Rapela (1995) interpreted rhyolites of the Marifil (V_1) and Chon Aike (V_2) formations to have been generated from andesitic parent magmas via multi-stage partial melting and fractionation. The parent andesite was generated by partial melting of 'Grenvillian' age lower crust. However, if the heat source for partial melting is related to basaltic underplating, the derivation of intermediate to silicic magmas with uniform isotope chemistry is better explained using the MASH (mixing, assimilation, storage and homogenization) hypothesis. We suggest that the process of deep crustal MASH, as defined by Hildreth & Moorbath (1988) was the dominant process in the lower crust of the proto-Pacific margin of Gondwana, leading to the development of intermediate to silicic magma with a uniform isotopic signature.

Basaltic underplating associated with subduction or mantle plume-related melting is interpreted to have induced lower-crustal melting. The MASH hypothesis predicts that the lower-crustal partial melts and mafic underplate mix, assimilate and homogenize. The magma would then crystallize or fractionate further to re-establish buoyant ascent. Compositionally, the magma would be andesite–dacite, and have a homogeneous 'base-level' isotopic signature, characteristic of that particular MASH domain. It is predicted from the close grouping of isotopic values that the MASH domain would have had a base-level isotopic signature of ~0·7070 ($^{87}Sr/^{86}Sr_i$) and ~−3 (εNd_i). Variations in this 'base-level' isotopic signature can be attributed to subtle differences in the MASH domain, or variable amounts of upper–middle-crustal contamination.

Although volcanic rocks from the Marifil (V_1), Mapple (V_2) and Chon Aike (V_2) formations have uniform Sr and Nd isotope compositions, close to the predicted values of the MASH domain, those of the Mount Poster and Brennecke formations have clearly undergone interaction with the middle–upper crust. A potential upper-crustal contaminant to account for the Mount Poster and Brennecke formation values would have to have strongly radiogenic $^{87}Sr/^{86}Sr$ and negative εNd (e.g. eastern Palmer Land paragneiss, $^{87}Sr/^{86}Sr_{185} = 0·7260$, $\varepsilon Nd_{185} =$

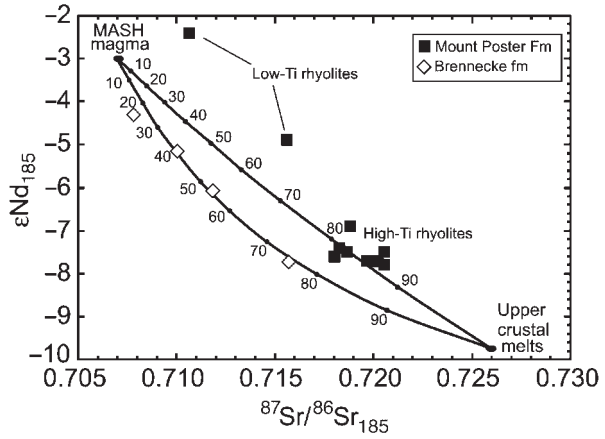

Fig. 9. εNd_i vs $^{87}Sr/^{86}Sr_i$ plot for Mount Poster and Brennecke formation rhyolites showing putative mixing curves. The MASH domain magma has $^{87}Sr/^{86}Sr_i = 0{\cdot}707$, $\varepsilon Nd_i = -3$ (see text) and Sr = 520 ppm, Nd = 25 ppm (average high-Ti rock from Mapple Formation). The upper-crustal melt component is taken from Palmer Land paragneiss (Wever *et al.*, 1994). The mixing curve for the Mount Poster Formation was calculated using the following parameters for the upper-crustal melt ($^{87}Sr/^{86}Sr_i = 0{\cdot}7260$, $\varepsilon Nd_i = 9{\cdot}75$, Sr = 175 ppm, Nd = 45 ppm), and for the Brennecke Formation ($^{87}Sr/^{86}Sr_i = 0{\cdot}7260$, $\varepsilon Nd_i = 9{\cdot}75$, Sr = 150 ppm, Nd = 80 ppm).

$-9{\cdot}7$; Wever *et al.*, 1994). Simple mixing between Palmer Land paragneiss and the MASH domain magma could lead to the compositions observed in the Mount Poster Formation (Fig. 9), although levels of contamination would have to be impossibly high (>70%). Such levels of contamination create many problems in terms of thermal budget, such that the magma will 'freeze', given the cooling effects of large amounts of assimilation. An alternative mechanism is that the MASH domain magma has mixed with melts of the upper–middle crust. The mixing line of Fig. 9 would still apply, and mixing between two magma types would not present the thermal problems that high levels of crustal contamination create. In the case of the Mount Poster Formation, the silicic rocks are much closer to melts of the upper crust, with only a small component of MASH domain magma (Fig. 9). Silicic volcanic rocks of the Brennecke Formation fall on a lower mixing line (Fig. 9), modelled by employing slightly different Sr and Nd contents for the crustal melt (Sr = 150 ppm, Nd = 80 ppm).

The isotopic differences between the high- and low-Ti thyolites are thought to result from their different geological setting. The high-Ti rhyolites have a small isotopic range ($^{87}Sr/^{86}Sr_{185} = 0{\cdot}7180$–$0{\cdot}7206$; $\varepsilon Nd_{185} = -6{\cdot}9$ to $-7{\cdot}8$; eight samples), whereas the low-Ti rhyolites have a range of $^{87}Sr/^{86}Sr_{185} = 0{\cdot}7106$–$0{\cdot}7156$; $\varepsilon Nd_{185} = -2{\cdot}4$ to $-4{\cdot}9$ (two samples). The high-Ti rhyolites are all intracaldera and are presumed to have developed in an upper-crustal magma chamber involving long-term mixing between upper-crustal melts and MASH magma, which facilitated the development of a relatively uniform, but strongly enriched isotope signature. The low-Ti rhyolites from outside the caldera setting are presumed to have followed a different evolutionary history outside the main magma chamber. They probably represent upper-crustal melts of a heterogeneous source, which mixed with MASH domain magma, but did not achieve homogenization in a large-scale convecting magma chamber (see Poitrasson & Pin, 1998).

Middle Jurassic volcanic rocks (V_2)

Silicic volcanic rocks from the Mapple Formation have been divided on the basis of major and trace element abundances into high- and low-Ti groups, and further divided on the basis of isotopic ratios. The high-Ti group includes andesite–dacite rock types, whereas the low-Ti group is dominated by rhyolites. Three isotopic subgroups have also been recognized, which have distinctive Sr, Nd and O isotopic characteristics (Table 4). The high- and low-$^{87}Sr/^{86}Sr$ subgroups comprise only the low-Ti group of rhyolites, whereas the mid-$^{87}Sr/^{86}Sr$ subgroup includes rocks from both the high- and low-Ti groups.

It is predicted from the close grouping of isotopic values (Table 2 and Fig. 8b), that the MASH domain (see V_1 petrogenesis) would have had a base-level isotopic signature of $^{87}Sr/^{86}Sr_i \sim 0{\cdot}707$ and $\varepsilon Nd_i \sim -3$. The oxygen isotopic signature is more difficult to define, given its total range from 6·1 to 10·6‰ ($\delta^{18}O_{quartz}$) in the Mapple Formation. The range corresponds to magma values of $\sim$5·1–9·6‰, as $\Delta_{quartz-melt}$ is ~ -1‰; therefore rhyolite melt values would be 1‰ lower than phenocryst value (Harris *et al.*, 1990). Possible reasons for this variation are as follows:

(1) source variation, but this is unlikely given the MASH hypothesis, where uniform $\delta^{18}O$ would also be expected.

(2) Variable upper-crustal contaminatiom, such that the $\delta^{18}O$ 'base-level' signature is $\sim$5‰, and all elevated values have been contaminated by middle–upper crust, which typically has values of <15‰ (Fowler & Harmon, 1990). A reasonable correlation between $\delta^{18}O$ and $^{87}Sr/^{86}Sr_{168}$ (Fig. 10) is also consistent with upper-crustal contamination. However, trace element contents (e.g. Ce/Yb, Ba, Sr) all suggest lower-crustal affinities. There is also the problem that the isotopic subgroups do not show uniform $\delta^{18}O$ values (with the exception of the high-$^{87}Sr/^{86}Sr$ subgroup), which would be anticipated if each subgroup had undergone different levels of interaction with upper–middle-crustal rocks. The problems associated with upper–middle-crustal contamination lend support to an alternative hypothesis to explain the range in $\delta^{18}O$.

(3) The primary 'base-level' $\delta^{18}O$ isotopic signature is closer to 10‰, typical of partial melts of granulitic lower

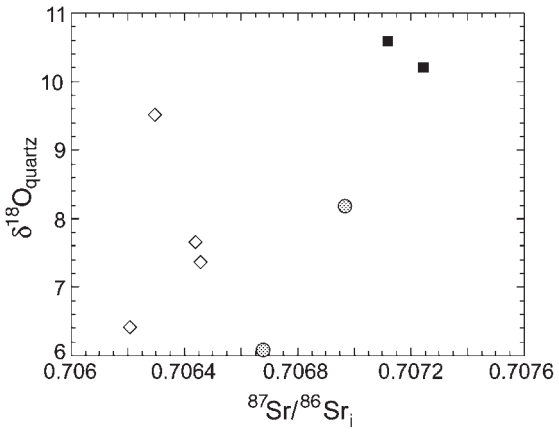

Fig. 10. $\delta^{18}O_{quartz}$ vs $^{87}Sr/^{86}Sr_{168}$ plot for high- (■), mid- (shaded circles) and low-$^{87}Sr/^{86}Sr_{168}$ (◇) rhyolites from the Mapple Formation.

crust (Fowler & Harmon, 1990). Very similar values have been determined (Harris *et al.*, 1990) on low-Ti rhyolites from the Paraná volcanic province (10·1–10·7‰) and the Etendeka volcanic province (9·7–11·2‰) also using mineral (pyroxene and plagioclase) separates to avoid known problems associated with low-temperature alteration (Harris *et al.*, 1990). These high values led Harris *et al.* (1990) and Harris & Milner (1997) to suggest an origin of lower-crustal melting for the low-Ti silicic rocks of the Paraná–Etendeka. The high $\delta^{18}O$ values also agree with the field defined by Molzahn *et al.* (1996) for lower-crustal xenoliths from the Transantarctic Mountains. Three of the eight samples analysed (Table 2) still preserve this signature ($\delta^{18}O_{quartz}$ = 9·5–10·6‰), whereas those with lower $\delta^{18}O$ values are thought to reflect interaction between the MASH domain cooling magma and meteoric water penetrating to mid-crustal levels (see Yardley & Valley, 1994), causing variable lowering of $\delta^{18}O_{magma}$ (see Harris & Erlank, 1992) without altering $^{87}Sr/^{86}Sr$ and εNd. The variable $\delta^{18}O_{quartz}$ values are not considered to be the result of late-stage, low-temperature alteration, which may alter the $\delta^{18}O$ whole-rock value, but would not alter the $\delta^{18}O$ value of quartz phenocrysts (Taylor, 1968).

Silicic rocks from the Chon Aike Formation also have remarkably uniform $^{87}Sr/^{86}Sr$ values (0·7067 ± 0·0005; 30 analyses; Pankhurst & Rapela, 1995), although they exhibit a slightly broader range in εNd (−1·8 to −3·9) and suggest the MASH domain was widespread throughout southern South America and the Antarctic Peninsula.

Relationship between $^{87}Sr/^{86}Sr$ subgroups and crustal contamination

The three $^{87}Sr/^{86}Sr$ subgroups (Table 4) are each characterized by uniform $^{87}Sr/^{86}Sr$ ratios, but show significant variation in SiO_2, Sr and Zr. The composition of the MASH domain magma is predicted to be andesite–dacite, given basaltic underplating into mafic lower crust (Hildreth & Moorbath, 1988); however, the volcanic rocks of the Mapple and Chon Aike formations are dominated by rhyolitic ignimbrites, with only rare intermediate rocks, and mafic rocks are absent. The occurrence of low- and high-Ti group rocks in the mid-$^{87}Sr/^{86}Sr$ subgroup of the Mapple Formation provides a test for the derivation of the silicic rocks from the andesites. The mid-$^{87}Sr/^{86}Sr$ subgroup is characterized by intermediate to silicic rocks (61–75 wt % SiO_2), all with uniform $^{87}Sr/^{86}Sr_{168}$ (∼0·7067) and εNd_{168} (∼−2·5). There is also a progressive decrease in Sr contents from ∼450 ppm to 150 ppm, coupled with increasing SiO_2. Such characteristics are likely to indicate (1) closed system fractionation from andesite to dacite and rhyolite, or (2) AFC that involves an assimilant with little isotopic contrast with that of the andesite magma. Closed system fractionation in the mid-$^{87}Sr/^{86}Sr$ subgroup was modelled using the Rayleigh fractionation equation, employing partition coefficient data summarized in Table 5 [taken from Rollinson (1993) and Thorpe *et al.* (1993)]. Using a fractionation assemblage of 55% plagioclase, 15% clinopyroxene, 20% orthopyroxene and 10% oxides [determined using the methods of Wright & Doherty (1970)], the high-SiO_2 (∼67%) rocks of the high-Ti group can be successfully derived from the low-SiO_2 rocks (SiO_2 ∼60–63%) via ∼20–25% crystallization. The low-Ti group rhyolites of the mid-$^{87}Sr/^{86}Sr$ subgroup, which have SiO_2 contents of >70%, can also be successfully modelled using a fractionating assemblage of plagioclase (50%), K-feldspar (15%), orthopyroxene (15%), magnetite (10%), quartz (10%) and zircon (<0·1%), by ∼40% fractional crystallization.

The two other $^{87}Sr/^{86}Sr$ subgroups contain only low-Ti rhyolites, and intermediate compositions are absent. Trace element abundances in the high-$^{87}Sr/^{86}Sr$ subgroup do not support a relationship involving fractional crystallization between the high- (74%) and low- (70%) SiO_2 rocks within this subgroup. All rocks are characterized by uniformly high Th (∼15 ppm), constant Eu/Eu*, and no obvious correlation with Sr or Ba, suggesting that feldspar-dominated fractionation was not important.

Although closed system crystal fractionation yields satisfactory results for generating the range of compositions seen in the mid-$^{87}Sr/^{86}Sr$ subgroup, a closed system process is geologically unlikely, as crustal interaction is almost inevitable. A more likely alternative to explain the data is that the MASH domain magma interacted with upper crust, both of which had similar isotopic compositions. If upper-crustal AFC processes were important we would expect to see reductions in Sr, development of negative Eu anomalies and increases in elements such as Pb and La/Nb ratios. Figure 11 shows the relationship between La/Nb and $^{87}Sr/^{86}Sr_{168}$ for the three subgroups. Within each isotopic subgroup there is

Table 5: Partition coefficients used in fractional crystallization model

	Plag	Cpx	Opx	Mt	Zircon
La	0·38	0·05	0·03		16·9
Ce	0·27	0·08	0·03	0·2	16·7
Nd	0·15	0·18	0·03		13·3
Sm	0·1	0·4	0·03	0·3	14·4
Eu	1·21	0·8	0·03	0·25	16
Gd	0·07	0·6	0·04		12
Tb					37
Yb	0·04	0·7	0·25	0·25	527
Lu	0·04	0·7	0·3		642
Y	0·06	1·5	0·45	0·5	
Th	0·01	0·01	0·05	0·1	62
Ta					55
Hf	0·02	0·2	0·1		2645
Zr	0·01	0·25	0·1	0·2	3479
Ti	0·05	0·4	0·25	20	
Sr	1·6	0·08	0·03	0·01	
Ba	0·16	0·03	0·01	0·01	
Rb	0·06	0·02	0·02	0·01	

Data from Rollinson (1993) and Thorpe *et al.* (1993).

little variation in $^{87}Sr/^{86}Sr_{168}$, but La/Nb shows a broad spread, strongly suggesting crustal assimilation with a contaminant that has a very similar $^{87}Sr/^{86}Sr$ ratio to that of the magma. Potential upper-crustal contaminants in the vicinity of the Mapple Formation are varied, and outcrop is scarce. To the north of the outcrop area of the Mapple Formation, Permo-Triassic metasedimentary rocks of the Trinity Peninsula Group crop out. Isotope compositions for the Trinity Peninsula Group ($^{87}Sr/^{86}Sr_{168}$ = 0·7065–0·7073; εNd_{168} = −2·6 to −4·2; Hole, 1986) fall within the range for the Mapple Formation. Other possible candidates are isolated outcrops of gneiss that crop out to the south of the Mapple Formation; the gneisses at Target Hill and Adie Inlet (Fig. 1b) have Rb–Sr whole-rock ages of ~420 Ma (Milne & Millar, 1989) and ~600 Ma (Pankhurst, 1983), respectively. The Adie Inlet gneiss has $^{87}Sr/^{86}Sr_{168}$ = 0·7070–0·7230 and εNd_{168} = −4·0 to −8·9 (Hole, 1986), and Target Hill has a range of $^{87}Sr/^{86}Sr_{168}$ = 0·7060–0·7075 and εNd_{168} = −1·5 to −3·9 (Milne, 1990), which fall within the range of Mapple Formation rhyolites. The upper-crustal rocks from eastern Graham Land all have an isotopic range that overlaps with that of the Mapple Formation volcanic rocks. As such, they could be responsible for causing small variations relative to the MASH domain 'base-level' signature and the variations

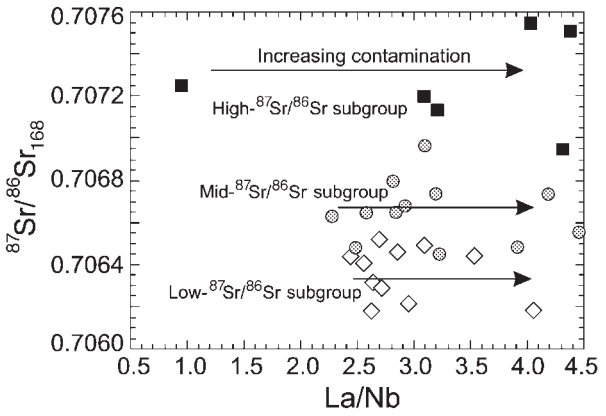

Fig. 11. $^{87}Sr/^{86}Sr_{168}$ vs La/Nb plot for high-, mid- and low-$^{87}Sr/^{86}Sr_{168}$ rhyolites from the Mapple Formation. The subgroups plot at fairly constant $^{87}Sr/^{86}Sr_{168}$, but show a broad spread in La/Nb, indicating contamination with crust that has similar $^{87}Sr/^{86}Sr_{168}$ isotopic values to that of the MASH magma.

in major and trace elements without concomitant changes to the isotopic ratios.

Physically, the isotopic subgroups are interpreted to represent individual upper-crustal magma chambers. This is consistent with the field relationships, which indicate a limited geographical extent for each subgroup (e.g. high-$^{87}Sr/^{86}Sr$ subgroup is largely confined to the Mapple Glacier area), although there is overlap between subgroups in most areas. It is also clear that individual magma chambers followed separate evolutionary paths from the same MASH domain magma, involving subtle differences in amount of assimilation and/or the nature of the assimilant.

An alternative mechanism to generate the rhyolites is upper-crustal anatexis of isotopically similar material (e.g. Trinity Peninsula Group metasedimentary rocks, Target Hill gneiss). However, the large volumes of rhyolite involved and the isotopic homogeneity over a very large area make upper-crustal anatexis unlikely.

PETROGENETIC MODEL

Several features of the silicic volcanic province may be critical in determination of a realistic petrogenetic model:

(1) each constituent formation was apparently erupted rapidly, and there were three main peaks of magmatism.

(2) The focus of magmatism migrated with time, such that the three episodes, V_1, V_2 and V_3, do not overlap in time or geographically.

(3) The province is overwhelmingly silicic (>70 wt % SiO_2). Basaltic rocks are absent, but some intermediate rocks do occur.

(4) Uniform Sr and Nd isotope ratios are widespread both spatially and chronologically. This is interpreted to

represent the development of a MASH domain magma, resulting from mixing between fractionated mafic underplate and partial melts of 'Grenvillian age' mafic lower crust. The V_1 silicic rocks of the southern Antarctic Peninsula are melts of upper-crustal paragneiss mixed with a minor component of MASH domain magma.

(5) The rhyolites have trace element characteristics of subduction-related magmas inherited from their source, although this is weaker in V_1 than in V_2 and V_3.

Subduction zone settings are characterized by the recycling of water into the mantle, and it is the presence of water that is a contributory factor for partial melting in the mantle wedge to produce arc magmas (e.g. Stolper & Newman, 1992; Tatsumi & Eggins, 1995). The detection of water in back-arc basins, large distances from the arc (Pearce *et al.*, 1995*b*), indicates that the 'water-assisted' generation of mantle partial melts will occur across a broad region, adjacent to the arc. It follows that the crust overlying the subduction zone will, over a period of time, become extensively intruded by hydrous, mantle-derived magmas, even if it is located to the rear of the volcanic front. A large proportion of such magmas are expected to collect in the lower crust, generating a hydrous, amphibole-rich, mafic layer at the point(s) where they freeze, because of density or thermal contrasts. During the Early Jurassic, or possibly earlier, we propose that such conditions were initiated in the lower crust of eastern Patagonia and the southern Antarctic Peninsula some distance from the arc. Experimental studies allow estimation of the conditions of partial melting of such material. At 10–13 kbar, the solidus of mafic amphibolite containing $\sim$1% H_2O is $\sim$800–920°C (Rushmer, 1991, 1993). Partial melting of amphibolite will generate silicic to intermediate compositions (55–75 wt % SiO_2) at temperatures of 1000–1050°C, at 8 kbar, representing partial melting of up to 25% (Rapp & Watson, 1995). The partial melting of hydrous mafic lower crust could have been initiated in response to extension, occurring without too much additional heat input (Pankhurst & Rapela, 1995), or by advection of mantle-derived heat by intrusion of basalt. Lower-crustal temperatures in arc environments are thought to be much less than 1000°C (e.g. Tatsumi & Eggins, 1995). It is therefore likely that melting was initiated by heating associated with the underplating of basaltic magma related to the peripheral effects of the mantle plume group responsible for the Karoo lavas (Discovery–Shona–Bouvet group; Storey *et al.*, 2001). The progression of silicic volcanism from NE to SW in Patagonia and south to north in the Antarctic Peninsula has been attributed to spreading of magmatism away from the plumes (Pankhurst *et al.*, 2000), taking into account palaeo-positions at the time of Gondwana break-up. At the onset of intrusion, mafic magmas are likely to be trapped at the base of the continental crust as a result of their density contrast, especially if the magmas have high *mg*-numbers, in equilibrium with mantle peridotite. Partial melting of the lower crust to generate zones of intermediate–silicic magma will reinforce this 'barrier', because the mafic melts cannot migrate through the less dense intermediate–silicic melt body (Huppert & Sparks, 1988). At this stage, partial melts of hydrous mafic lower crust can mix with fractionates of the basaltic underplate, leading to the development of the isotopically homogeneous MASH domain magma. Further intrusion of mafic melts will pond, lead to continued intermediate–silicic magma generation and subsequent mixing, such that a 'runaway' system can develop whereby the continued intrusion (underplating) of mafic magma leads to increased intermediate–silicic melt, which further reduces the possibility of unfractionated mafic melt escaping upward through the crust.

The onset of silicic volcanism is preceded by the upward transport of intermediate–silicic melts through dykes, driven by density contrasts within the crust (Clemens & Mawer, 1992; Petford *et al.*, 1994; Weinberg, 1999). This will lead to the development of upper-crustal magma chambers and subsequent high rates of eruption predicted for the silicic rocks. Residence in upper-crustal magma chambers allows interaction with upper-crustal rocks, probably via AFC, causing alteration to the isotopic composition of the MASH domain magma. The cessation of silicic magmatism would result from reduced heat input and slow cooling of the crust. Large volume silicic melt generation may have consumed the fusible part of the lower crust; therefore restricting spatial overlap between silicic formations. The episodic nature of the magmatism reflects the thermal migration away from the plume source, and development of preconditions for silicic volcanism, which occurs over a few million years before rapid eruption of the silicic rocks.

CONCLUSIONS

(1) A major silicic province developed along the proto-Pacific margin of Gondwana, marked by three main episodes (Pankhurst *et al.*, 2000) of rhyolite ignimbrite-dominated volcanism: V_1 (188–178 Ma), V_2 (172–167 Ma) and V_3 (162–153 Ma). The silicic province extends for >3000 km along the proto-Pacific margin, cropping out in Patagonian South America and the Antarctic Peninsula.

(2) The silicic province developed during the early stages of Gondwana break-up and was, in part, contemporaneous with the vast basaltic outpourings of the Karoo and Ferrar ($\sim$182 Ma; Duncan *et al.*, 1997).

(3) The Middle Jurassic silicic rocks of the Mapple Formation (Antarctic Peninsula) and those of the Chon Aike Formation (South America) are thought to have been generated as a result of anatexis of 'Grenvillian age' hydrous mafic lower crust, linked to pre-Middle Jurassic,

arc-related underplating. The lower-crustal partial melts would have mixed with fractionated components of the mafic underplate and long-term storage would have led to the development of an isotopically uniform MASH domain magma ($^{87}Sr/^{86}Sr_i \sim 0{\cdot}707$; $\varepsilon Nd_i \sim -3$). The parent composition is probably close to andesite–dacite, therefore the rhyolites are the result of AFC in upper-crustal magma chambers involving upper-crustal assimilants with similar isotopic composition to that of the magma. Early Jurassic (V_1) rocks of the Mount Poster and Brennecke formations are more isotopically enriched than the Middle Jurassic rocks, whereas the Marifil Formation rhyolites of Patagonia have an isotopic composition close to that of the MASH domain magma. The rhyolites of the Mount Poster and Brennecke formations are interpreted as melts of upper-crustal paragneiss ($^{87}Sr/^{86}Sr_{185} = 0{\cdot}7260$; $\varepsilon Nd_{185} = -9{\cdot}7$), which have mixed with the MASH domain component in upper-crustal magma chambers.

(4) Partial melting of the lower crust will be strongly influenced by the presence of hydrous, fusible crust derived from the mantle wedge. The generation of intermediate–silicic melts by partial melting of hydrous lower crust provides a 'barrier' to ascending mafic magma, such that continued mafic magmatism creates further heating of the lower crust, which causes increased intermediate–silicic melt production, reinforcing the 'barrier'. The development of large volumes of intermediate–silicic melt in the lower crust will escape, via dyking, to upper-crustal magma chambers, before short-lived pulses of large volume silicic magmatism. After cooling and exhaustion of the fusible part of the lower crust, silicic volcanism ceases. The migration of silicic volcanism through the Jurassic reinforces this, given that the V_1, V_2 and V_3 episodes do not overlap.

(5) The silicic province developed along the proto-Pacific margin of Gondwana in an extensional environment, which was almost certainly linked to the initial stages of continental break-up. Lower-crustal anatexis and MASH processes were in response to mafic underplating associated with the Discovery–Shona–Bouvet plume group, responsible for the Karoo magmatic province. The progression (old–young) of volcanism from NE to SW in Patagonia and south to north in the Antarctic Peninsula is consistent with migration of magmatism away from the mantle plume towards the proto-Pacific margin of Gondwana during rifting and break-up.

ACKNOWLEDGEMENTS

This paper has benefited greatly from the thoughtful reviews of Charles Bacon, David Peate and Marge Wilson, and comments on an earlier manuscript by Bryan Storey. The field and air operations staff at Rothera Base are thanked for their support. Julian Pearce (University of Durham) supplied the ICP-MS analyses, Dave Emley (University of Keele) carried out the XRF analyses, and the Foundation for Research & Development (South Africa) financed the O-isotope analysis.

REFERENCES

Aragón, E., Rodriguez, A. M. I. & Benialgo, A. (1996). A calderas field at the Marifil Formation, new volcanogenic interpretation, Norpatagonian Massif, Argentina. *Journal of South American Earth Sciences* **9**, 321–328.

Bacon, C. R., Foster, H. L. & Smith, J. G. (1990). Rhyolitic calderas of the Yukon–Tanana Terrane, east central Alaska—volcanic remnants of a mid-Cretaceous magmatic arc. *Journal of Geophysical Research* **95**, 21451–21461.

Cameron, M., Bagby, W. C. & Cameron, K. L. (1980). Petrogenesis of voluminous mid-Tertiary ignimbrites of the Sierra Madre Occidental. *Contributions to Mineralogy and Petrology* **74**, 271–284.

Clemens, J. D. & Mawer, C. K. (1992). Granitic magma transport by fracture propagation. *Tectonophysics* **204**, 339–360.

Cleverly, R. W., Betton, P. J. & Bristow, J. W. (1984). Geochemistry and petrogenesis of the Lebombo rhyolites. *Geological Society of South Africa, Special Publication* **13**, 171–195.

Cox, K. G. (1992). Karoo igneous activity and the early stages of the break-up of Gondwanaland. In: Storey, B. C., Alabaster, T. & Pankhurst, R. J. (eds) *Magmatism and the Causes of Continental Break-up. Geological Society, London, Special Publications* **68**, 137–148.

Duncan, R. A., Hooper, P. R., Rehacek, J., Marsh, J. S. & Duncan, A. R. (1997). The timing and duration of the Karoo igneous event, southern Gondwan. *Journal of Geophysical Research* **102**, 18127–18138.

Ewart, A., Schön, R. W. & Chappell, B. W. (1992). The Cretaceous volcanic–plutonic province of the central Queensland (Australia) coast—a rift related 'calc-alkaline' province. *Transactions of the Royal Society of Edinburgh, Earth Sciences* **83**, 327–345.

Fanning, C. M. & Laudon, T. S. (1999). Mesozoic volcanism, plutonism and sedimentation in eastern Ellsworth Land, West Antarctica. *8th International Symposium on Antarctic Earth Sciences, Wellington, New Zealand, Abstracts*. Wellington: Royal Society of New Zealand, p. 102.

Féraud, G., Alric, V., Fornari, M., Bertrand, H. & Haller, M. (1999). $^{40}Ar/^{39}Ar$ dating of the Jurassic volcanic province of Patagonia: migrating magmatism relating to Gondwana break-up and subduction. *Earth and Planetary Science Letters* **172**, 83–96.

Floyd, P. A. (1985). Petrology and geochemistry of intraplate sheet-flow basalts, Nauru Basin, Deep Sea Drilling Project leg 89. In: Moberley, R. & Schlanger, S. O. (eds) *Initial Reports of the Deep Sea Drilling Project, 89*. Washington, DC: US Government Printing Office, pp. 471–497.

Fowler, M. B. & Harmon, R. S. (1990). The oxygen isotope composition of lower crustal granulite xenoliths. In: Vielzeuf, D. & Vidal, P. (eds) *Granulites and Crustal Evolution*. Dordrecht: Kluwer Academic, pp. 493–506.

Garland, F., Hawkesworth, C. J. & Mantovani, S. M. (1995). Description and petrogenesis of the Parana rhyolites, southern Brazil. *Journal of Petrology* **36**, 1193–1227.

Harris, C. & Erlank, A. J. (1992). The production of large-volume, low-$\delta^{18}O$ rhyolites during the rifting of Africa and Antarctica: the Lebombo Monocline, southern Africa. *Geochimica et Cosmochimica Acta* **56**, 3561–3570.

Harris, C. & Milner, S. (1997). Crustal origin for the Paraná rhyolites: discussion of 'Description and petrogenesis of the Paraná rhyolites,

southern Brazil' by Garland *et al.* (1995). *Journal of Petrology* **38**, 299–302.

Harris, C., Whittingham, A. M., Milner, S. C. & Armstrong, R. A. (1990). Oxygen isotope geochemistry of the Karoo and Etendeka volcanic provinces of southern Africa. *South African Journal of Geology* **98**, 126–139.

Hildreth, W. & Moorbath, S. (1988). Crustal contributions to arc magmatism in the Andes of central Chile. *Contributions to Mineralogy and Petrology* **98**, 455–489.

Hole, M. J. (1986). Time controlled geochemistry of igneous rocks of the Antarctic Peninsula. Ph.D. thesis, University of London.

Hole, M. J. (1988). Post-subduction alkaline volcanism along the Antarctic Peninsula. *Journal of the Geological Society, London* **145**, 985–998.

Howells, M. F., Reedman, A. F. & Campbell, S. D. G. (1991). *Ordovician (Caradoc) Marginal Basin Volcanism in Snowdonia (NW Wales)*. London: HMSO for the British Geological Survey, 191 pp.

Huppert, H. E. & Sparks, R. S. J. (1988). The generation of granitic magmas by intrusion of basalt into continental crust. *Journal of Petrology* **29**, 599–624.

Kellogg, K. S. & Rowley, P. D. (1989). Structural geology and tectonics of the Orville Coast region, southern Antarctic Peninsula, Antarctica. *US Geological Survey, Professional Paper* **1498**.

Leat, P. T., Scarrow, J. H. & Millar, I. L. (1995). On the Antarctic Peninsula batholith. *Geological Magazine* **132**, 399–412.

Lipman, P. W. (1984). The roots of ash-flow calderas in western North America: windows into the tops of granitic batholiths. *Journal of Geophysical Research* **89**, 8801–8841.

Macdonald, R., Smith, R. L. & Thomas, J. E. (1992). Chemistry of the subalkalic silicic obsidian. *US Geological Survey, Professional Paper* **1523**, 214 pp.

McCulloch, M. T., Kyser, T. K., Woodhead, J. D. & Kinsley, L. (1994). Pb–Sr–Nd–O isotopic constraints on the origin of rhyolites from the Taupo volcanic zone of New Zealand: evidence for assimilation followed by fractionation from basalt. *Contributions to Mineralogy and Petrology* **115**, 303–312.

Milne, A. J. (1990). The pre-Mesozoic geological evolution of Graham Land, Antarctica. Ph.D. thesis, Open University, Milton Keynes.

Milne, A. J. & Millar, I. L. (1989). Short paper: The significance of mid-Palaeozoic basement in Graham Land, Antarctic Peninsula. *Journal of the Geological Society, London* **146**, 207–210.

Molzahn, M., Reisberg, L. & Wörner, G. (1996). Os, Sr, Nd, Pb, O isotope and trace element data from the Ferrar flood basalts, Antarctica: evidence for an enriched subcontinental lithospheric source. *Earth and Planetary Science Letters* **144**, 529–546.

Nakamura, N. (1974). Determination of REE, Ba, Fe, Mg, Na and K in carbonaceous and ordinary chondrites. *Geochimica et Cosmochimica Acta* **38**, 757–773.

Pankhurst, R. J. (1982). Rb–Sr geochronology of Graham Land, Antarctic. *Journal of the Geological Society, London* **139**, 701–711.

Pankhurst, R. J. (1983). Rb–Sr constraints on the ages of basement rocks of the Antarctic Peninsula. In: Oliver, R. L., James, P. R. & Jago, J. B. (eds) *Antarctic Earth Science*. Cambridge: Cambridge University Press, pp. 367–371.

Pankhurst, R. J. & Rapela, C. R. (1995). Production of Jurassic rhyolites by anatexis of the lower crust of Patagonia. *Earth and Planetary Science Letters* **134**, 23–36.

Pankhurst, R. J., Leat, P. T., Sruoga, P., Rapela, C. W., Márquez, M., Storey, B. C. & Riley, T. R. (1998). The Chon Aike silicic igneous province of Patagonia and related rocks in Antarctica: a silicic large igneous province. *Journal of Volcanology and Geothermal Research* **81**, 113–136.

Pankhurst, R. J., Riley, T. R., Fanning, C. M. & Kelley, S. R. (2000). Episodic silicic volcanism in Patagonia and the Antarctic Peninsula: chronology of magmatism associated with the break-up of Gondwana. *Journal of Petrology* **41**, 605–625.

Pearce, J. A. (1982). Trace element characteristics of lavas from destructive plate boundaries. In: Thorpe, R. S. (ed.) *Andesites: Orogenic Andesites and Related Rocks*. Chichester: Wiley, pp. 525–548.

Pearce, J. A., Harris, N. B. W. & Tindle, A. G. (1984). Trace element discrimination diagrams for the tectonic interpretation of granitic rocks. *Journal of Petrology* **25**, 953–956.

Pearce, J. A., Baker, P. E., Harvey, P. K. & Luff, I. W. (1995*a*). Geochemical evidence for subduction fluxes, mantle melting and fractional crystallisation beneath the South Sandwich island arc. *Journal of Petrology* **36**, 1073–1109.

Pearce, J. A., Ernewein, M., Bloomer, S. H., Parson, L. M., Murton, B. J. & Johnson, L. E. (1995*b*). Geochemistry of Lau Basin volcanic rocks: influence of ridge segmentation and arc proximity. In: Smellie, J. L. (ed.) *Volcanism Associated with Extension at Consuming Plate Margins*. *Geological Society, London, Special Publications* **81**, 53–76.

Petford, N., Lister, J. R. & Kerr, R. C. (1994). The ascent of felsic magmas in dykes. *Lithos* **32**, 161–168.

Poitrasson, F. & Pin, C. (1998). Extreme Nd isotope homogeneity in a large rhyolitic province: the Estérel massif, southeast France. *Bulletin of Volcanology* **60**, 213–223.

Rapela, C. W. & Pankhurst, R. J. (1993). El volcanismo ríolitico del noreste de la Patagonia: un evento meso-jurásico de corta duración y origen profundo. *Actas del XII Congreso Geológico Argentino, Mendoza* **4**, 179–188.

Rapp, R. P. & Watson, E. B. (1995). Dehydration melting of metabasalt at 8–32 kbar: implications for continental growth and crust–mantle recycling. *Journal of Petrology* **36**, 891–932.

Riley, T. R. & Leat, P. T. (1999). Large volume silicic volcanism along the proto-Pacific margin of Gondwana: lithological and stratigraphical investigations from the Antarctic Peninsula. *Geological Magazine* **136**, 1–16.

Riley, T. R., Crame, J. A., Thomson, M. R. A. & Cantrill, D. J. (1997). Late Jurassic (Kimmeridgian–Tithonian) macrofossil assemblage from Jason Peninsula, Graham Land: evidence for a significant northward extension of the Latady Formation. *Antarctic Science* **9**, 434–442.

Rollinson, H. (1993). *Using Geochemical Data: Evaluation, Presentation, Interpretation*. Harlow, UK: Longman, 352 pp.

Rowley, P. D., Schimdt, D. L. & Williams, P. L. (1982). Mount Poster Formation, southern Antarctic Peninsula and eastern Ellsworth Land. *Antarctic Journal of the United States* **17**, 38–39.

Rushmer, T. (1991). Partial melting of two amphibolites: contrasting experimental results under fluid-absent conditions. *Contributions to Mineralogy and Petrology* **107**, 41–59.

Rushmer, T. (1993). Experimental high-pressure granulites: some applications to natural mafic xenolith suites and Archean granulite terranes. *Geology* **21**, 411–414.

Smellie, J. L. (1991). Middle–Late Jurassic volcanism on the Jason Peninsula, Antarctic Peninsula, and its relationship to the break-up of Gondwana. In: Ulbrich, H. & Rocha Campos, A. C. (eds) *Gondwana 7 Proceedings*. São Paulo: Universidade de São Paulo, pp. 685–699.

Smellie, J. L., Roberts, B. & Hirons, S. R. (1996). Very low- and low-grade metamorphism in the Trinity Peninsula Group (Permo-Triassic) of northern Graham Land, Antarctic Peninsula. *Geological Magazine* **133**, 583–594.

Stewart, D. B. (1979). The formation of siliceous potassic glassy rocks. In: Yoder, H. S., Jr (ed.) *The Evolution of the Igneous Rocks*. Princeton, NJ: Princeton University Press, pp. 339–350.

Stolper, E. & Newman, S. (1992). The role of water in the petrogenesis of Mariana trough magmas. *Earth and Planetary Science Letters* **121**, 293–325.

Storey, B. C. & Garrett, S. W. (1985). Crustal growth of the Antarctic Peninsula by accretion, magmatism and extension. *Geological Magazine* **122**, 5–14.

Storey, B. C. & Kyle, P. R. (1997). An active mantle mechanism for Gondwana breakup. *South African Journal of Geology* **100**, 1–8.

Storey, B. C., Alabaster, T., Hole, M. J., Pankhurst, R. J. & Wever, H. E. (1992). Role of subduction plate boundary forces during the initial stages of Gondwana break-up: evidence from the proto-Pacific margin of Antarctica. In: Storey, B. C., Alabaster, T. & Pankhurst, R. J. (eds) *Magmatism and the Causes of Continental Break-up. Geological Society, London, Special Publications* **68**, 149–163.

Storey, B. C., Leat, P. T. & Ferris, J. K. (2001). The location of mantle plume centres during the initial stages of Gondwana break-up. In: Ernst, R. E. & Buchan, K. L. (eds) *Locating pre-Mesozoic Mantle Plumes. Geological Society of America, Special Paper* (in press).

Sun, S.-S. & McDonough, W. D. (1989). Chemical and isotopic systematics of oceanic basalts: implications for mantle composition and processes. In: Saunders, A. D. & Norry, M. J. (eds) *Magmatism in the Ocean Basins. Geological Society, London, Special Publications* **42**, 313–345.

Tatsumi, Y. & Eggins, S. (1995). *Subduction Zone Magmatism*. Oxford: Blackwell Science, 211 pp.

Taylor, H. P., Jr (1968). The oxygen isotope geochemistry of igneous rocks. *Contributions to Mineralogy and Petrology* **19**, 1–71.

Thomson, M. R. A. & Pankhurst, R. J. (1983). Age of post-Gondwanian calc-alkaline volcanism in the Antarctic Peninsula region. In: Oliver, R. L., James, P. R. & Jago, J. B. (eds) *Antarctic Earth Science*. Cambridge: Cambridge University Press, pp. 328–333.

Thompson, R. N., Morrison, M. A., Hendry, G. L. & Parry, S. J. (1984). An assessment of the relative roles of crust and mantle in magma genesis: an elemental approach. *Philosophical Transactions of the Royal Society of London, Series A* **310**, 549–590.

Thorpe, R. S., Leat, P. T., Mann, A. C., Howells, M. F., Reedman, A. J. & Campbell, S. D. G. (1993). Magmatic evolution of the Ordovician Snowdon volcanic centre, North Wales (UK). *Journal of Petrology* **34**(4), 711–741.

Weinberg, R. F. (1999). Mesoscale pervasive felsic magma migration: alternatives to dyking. *Lithos* **46**, 393–410.

Wever, H. E. & Storey, B. C. (1992). Bimodal magmatism in northeast Palmer Land, Antarctic Peninsula: geochemical evidence for a Jurassic ensialic back-arc basin. *Tectonophysics* **205**, 239–259.

Wever, H. E., Millar, I. L. & Pankhurst, R. J. (1994). Geochronology and radiogenic isotope geology of Mesozoic rocks from eastern Palmer Land, Antarctic Peninsula: crustal anatexis in arc-related granitoid genesis. *Journal of South American Earth Sciences* **7**, 69–83.

White, R. S. & McKenzie, D. (1989). Magmatism at rift zones: the generation of volcanic continental margins and flood basalts. *Journal of Geophysical Research* **94**, 7685–7729.

Wright, T. L. & Doherty, P. C. (1970). A linear programming and least squares computer method for solving petrologic mixing problems. *Geological Society of America Bulletin* **81**, 1995–2008.

Yardley, B. W. D. & Valley, J. W. (1994). How wet is the Earth's crust? *Nature* **371**, 205–206.